iScience

CellPress

Article

Induction of Inflammatory Macrophages in the Gut and Extra-Gut Tissues by Colitis-Mediated *Escherichia coli*

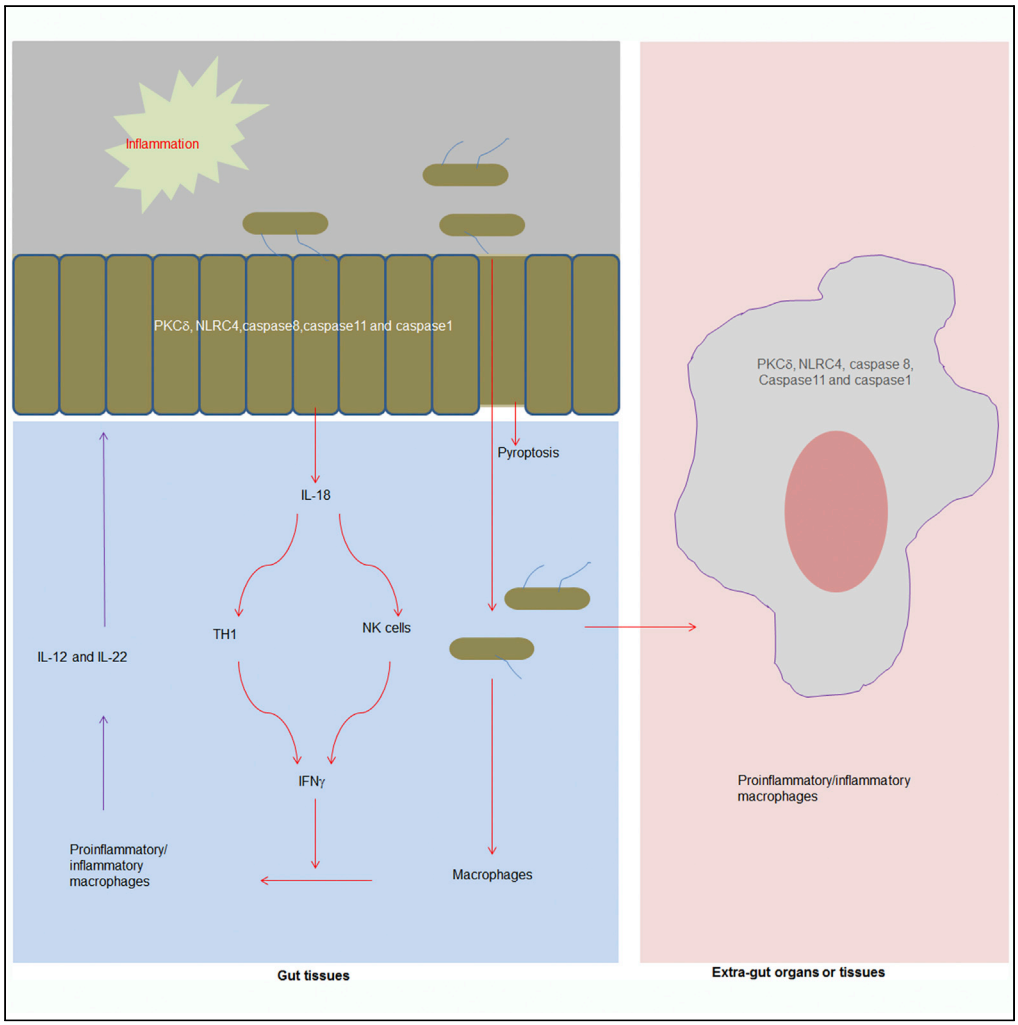

Houbao Qi, Yunhuan Gao, Yuanyuan Li, ..., Yanmei Xu, Yuan Zhang, Rongcun Yang

ryang@nankai.edu.cn

HIGHLIGHTS

Increased commensal *E. coli* in colitis induce inflammatory macrophages

Colitic *E. coli* are different from other commensal and pathogenic *E. coli*

Gut inflammatory macrophages by *E. coli* need IL-18, IFN-γ, IL-12, and IL-22

PCKδ, NLRC4, caspase8, and caspase1/11 are required for *E. coli*-mediated activation

Qi et al., iScience *21*, 474–489 November 22, 2019
https://doi.org/10.1016/j.isci.2019.10.046

iScience

CellPress

Article

Induction of Inflammatory Macrophages in the Gut and Extra-Gut Tissues by Colitis-Mediated *Escherichia coli*

Houbao Qi,[1,2,3] Yunhuan Gao,[1,2,3] Yuanyuan Li,[1,2,3] Jianmei Wei,[1,2,3] Xiaomin Su,[1,2,3] Chunze Zhang,[4] Yingquan Liu,[1,2,3] Hua Zhu,[5] Lei Sui,[5] Yanwen Xiong,[6] Xi Yang,[6] Yanmei Xu,[6] Yuan Zhang,[1,2,3] and Rongcun Yang[1,2,3,7,*]

SUMMARY

Inflammatory macrophages play a critical role in gut and extra-gut inflammatory disorders, which may be promoted through the dysbiosis of gut microbiota. However, it is poorly understood how gut microbiota affect inflammatory macrophages. Here, we found that increased *Escherichia coli (E. coli)* in inflamed colon may induce inflammatory macrophages in gut and extra-gut tissues. These *E. coli* are different from other commensal and pathogenic *E. coli* in genomic components and also in ability to induce inflammatory responses. Dominant *E. coli* from colitic tissues induce gut inflammatory macrophages through a regulating network consisted of IL-18, IFN-γ, IL-12, and IL-22 in gut tissues. These *E. coli* also directly activate macrophages. Cytosolic inflammasome components PCKδ, NLRC4, caspase8, and caspase1/11 are involved in *E. coli*-mediated activation in both gut epithelial cells and macrophages. These disclose a novel mechanism for how dysbiosis of gut microbiota in colitis cause inflammatory macrophages related to multiple diseases.

INTRODUCTION

The dysbiosis (aberrant gut microbiota composition and function) of gut microbiota may promote gut and extra-gut autoimmune and inflammatory disorders such as inflammatory bowel disease (IBD), obesity, atherosclerosis, carcinogenesis, etc (Blander et al., 2017). Although the mechanisms involved are not well understood, the inflammatory macrophages have a causal association with these diseases (Sekirov et al., 2010; Wynn et al., 2013). Thus it is critical to understand how gut microbiota regulate these macrophages.

Tissue-resident macrophages represent a highly heterogeneous cell population able to sense and quickly adapt to environmental cues such as gut tissue macrophages, which play either protective or tolerogenic roles. In steady state conditions, the gut lamina propria (LP) macrophages display an anergic phenotype and are essential for intestinal homeostasis (De Schepper et al., 2018); but under inflammatory settings such as DSS-mediated colitis, the conditioning of murine Ly6C$^+$ blood monocytes is impaired, and they give rise to inflammatory macrophages (Zigmond et al., 2012). These inflammatory macrophages produce large amounts of mediators such as TNFα, IL6, IL-1β, reactive oxygen intermediaries, and nitric oxide to cause diseases (MacDonald et al., 2011). Thus, the transformation of suppressive macrophages back into proinflammatory phenotype or inflammatory macrophages into anti-inflammatory cells has a major impact on the progression and resolution of the inflammation-associated diseases. It is unclear how the transformation of these macrophages is induced and maintained in these diseases. Alterations in the microbiome population and/or changes in gut permeability may promote microbial translocation into the distal tissues and/or organs. Danger signals derived from the microbiome can trigger the inflammatory cascade and activate macrophages to transform into inflammatory macrophages. However, what danger signal(s) of gut microbiota induce inflammatory macrophages remains poorly understood.

Certain members of the microbiota have been linked to inflammatory responses and intestinal pathology in mouse models such as that the members of the *Enterobacteriaceae* family, *Klebsiella pneumoniae* and *Proteus mirabilis* (Garrett et al., 2010). *Enterobacteriaceae* act in concert with the gut microbiota to induce spontaneous and maternally transmitted colitis (Garrett et al., 2010). *E. coli*, another member of *Enterobacteriaceae* family, is present in very less proportion in gut contents under normal physiological conditions (Schieber et al., 2015). However, a high abundance of commensal *E. coli* (facultative anaerobic

[1]State Key Laboratory of Medicinal Chemical Biology, Nankai University, Tianjin 300071, China

[2]Key Laboratory of Bioactive Materials Ministry of Education, Nankai University, Tianjin 300071, China

[3]Department of Immunology, Nankai University School of Medicine, Nankai University, Tianjin 300071, China

[4]Department of Colorectal Surgery, Tianjin Union Medical Center, Tianjin 300121, China

[5]Key Laboratory of Human Disease Comparative Medicine, Ministry of Health, Institute of Laboratory Animal Science, Chinese Academy of Medical Sciences (CAMS) Comparative Medical Center, Peking Union Medical College (PUMC), Beijing 100021, China

[6]Collaborative Innovation Center for Diagnosis and Treatment of Infectious Diseases, State Key Laboratory of Infectious Disease Prevention and Control, National Institute for Communicable Disease Control and Prevention, Chinese Center for Disease, Control and Prevention, 155 Changbai Road, Changping District, Beijing 102206, China

[7]Lead Contact

*Correspondence: ryang@nankai.edu.cn

https://doi.org/10.1016/j.isci.2019.10.046

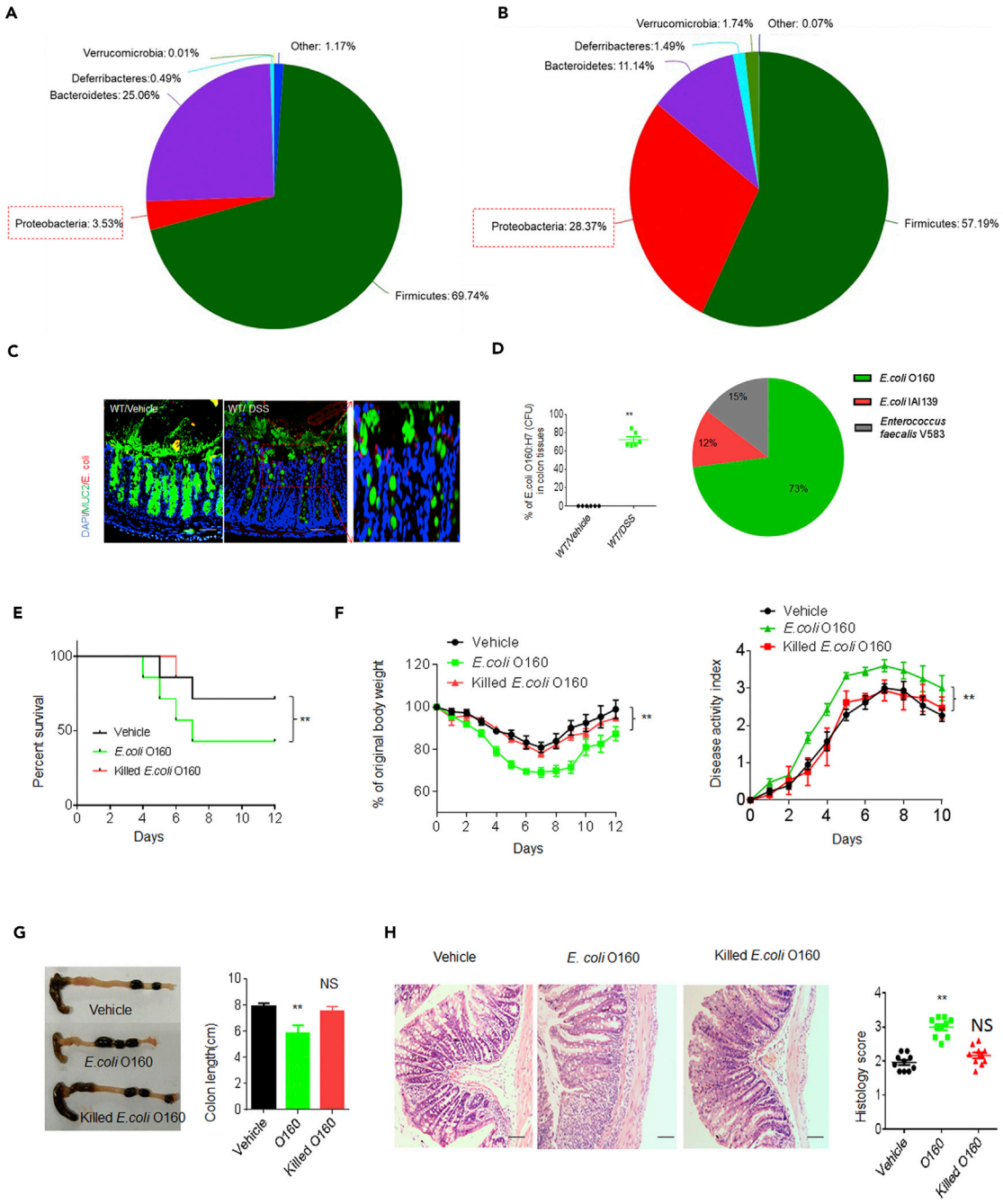

Figure 1. Characteristics of *E. coli* O160:H7 Isolated from Inflamed Colon Tissues

(A and B) 16s rDNA analyses of colon contents in DSS-treated wt (male, n = 5) and un-molested control mice (male, n = 5). The samples were clustered at phylum levels using the sample phylum count matrices and composition of colon bacteria (phylum levels) in control (A) and DSS-treated (B) mice. Mice were fed a 2.5% DSS solution in drinking water for 7 days.

(C) Fluorescent *in situ* hybridization (FISH) of *E. coli* in colon tissues of DSS-treated and un-molested mice (one representative, n = 6). Red, *E. coli*; Green, mucus; Blue, nuclei.

(D) Percent of *E. coli* O160:H7 clones in colitic tissues. The bacteria from colon tissues of DSS-treated and un-molested mice were *in vitro* cultured and then CFU of bacteria were sequenced through V1-V9 regions (n = 6).

(E and F) Survival rate (E), body weight, and disease activity index (F) in DSS-treated mice infused by *E. coli* O160:H7, heat-killed dead (killed) *E. coli* O160:H7, and *E. coli* IAI39 (isolated from mice by us) (n = 12). Mice were treated using pan-antibiotics for one week before infusing *E. coli*. Data in F are represented as mean ± SD.

(G) Length of colon were monitored at day 7 after DSS. Data are represented as mean ± SD.

Figure 1. *Continued*

(H) H&E staining and histological scores of colon tissues in DSS-treated mice infused by *E. coli* O160:H7 killed *E. coli* O160:H7. Scale bars = 40 μm. Data are represented as mean ± SD.

Two-side student's *t*-test in D; Kruskal Wallis test in E; analysis of variance test in F; ANOVA plus post-Bonferroni analysis in G and H; *p<0.05, **p<0.01, and ***p<0.001; NS, no significance. Data in D and H are represented as mean ± SEM. Data in F and G are represented as mean ± SD. Data in E–H are a representative of three independent experiments. See also Figure S1, Table S1, and https://www.ncbi.nlm.nih.gov/sra/PRJNA512937.

Proteobacteria in phylum and *Enterobacteriaceae* in genus) is commonly observed during inflammation in the colon (Winter and Baumler, 2014), including chemically induced colitis, antibiotic-treated mice, infection with enteric pathogens, and genetically induced colitis (Winter and Baumler, 2014). Microbial communities in patients with inflammatory bowel diseases also exhibit an increased prevalence of *E. coli* (Winter and Baumler, 2014). However, the physiological and pathological function(s) of these *E. coli* are poorly understood. One isolated *E. coli* strain from antibiotic-treated mice may cause lethal inflammasome activation (Ayres et al., 2012), whereas another strain *E. coli* may protect mice against muscle wasting and loss of fat during enteric *Salmonella typhimurium* or respiratory Burkholderia thailandensis infections (Schieber et al., 2015). Here, we found that a high abundance of commensal *E.coli* in inflamed colon not only indirectly induce inflammatory macrophages through gut epithelial cells but also directly activate extra-gut macrophages through cytosolic inflammasome complexes consisted of PCKδ (phosphoenolpyruvate carboxykinase δ), NLRC4 (NLR family CARD domain-containing protein 4), caspase8, and caspase1/11. These inflamed tissues derived *E. coli* do not cause acute disease symptoms.

RESULTS

E. coli O160:H7 Isolated from Inflamed Colon Promotes Sensitivity to DSS-mediated Colitis

To characterize inflammation-mediated *E. coli*, we employed chemically induced colitis (dextran sulfate sodium [DSS]-mediated colitis), in which there is a relative luminal abundance of *Proteobacteria* phylum (*Enterobacteriaceae* genus, *E. coli* species) (Schieber et al., 2015). Consistent with this report, the increased gut *Proteobacteria* phylum, *Enterobacteriaceae* genus, and *E. coli* was detected in the colonic contents and tissues of DSS-treated mice (Figures 1A and 1B and https://www.ncbi.nlm.nih.gov/sra/PRJNA512937). Using culturing techniques, serotyping, and genetic and molecular characterization, we identified a dominant *E. coli* strain from these inflamed colon tissues, named as *E.coli* O160:H7 strain (Figures S1A–S1C, 1C, and 1D, Table S1A and http://www.ncbi.nlm.nih.gov/bioproject/513139). *E. coli* O160:H7 strain was also present in the microbiota of unmanipulated mice but was not abundant, suggesting it is not able to compete efficiently for intestinal colonization. We next sequenced the genome of *E. coli* O160:H7 isolate and aligned the reads to reference *E. coli* genomes (Table S1B). The composition of *E. coli* O160:H7 gene clusters was different from other pathogenic *E. coli* O157:H7 and *E. coli* CFT073 and also unpathogenic *E. coli* str.k12 substr.MG1655 (Figures S1B and S1C). The *fliC* gene, encoding flagellin (H-antigen), was similar to that of *E. coli* O157:H7 isolates (Figure S1D). But, type III secretion system (T3SS) of *E. coli* O160:H7 was different from pathogenic *E. coli* O157.H7 such that T3SS of *E. coli* O160:H7 contained *hxlB*, *irp1*, *HMWP1*, *pqqL*, *hokA*, *fhaB*, *fdoG*, *fdfH*, *ttuB*, *bax*, *PTS-Dga*, *EIID*, *dgaD*, *glmS*, *GFPT*, *ABC-2*, and *CPSE.A*, which were not detected in *E. coli* O157:H7 (Table S1C). Notably, we did not find virulence-related membrane protein genes such as *enterotoxin*, *EspB*, *EspA*, *SepZ*, *SepD*, *Hcp-like protein*, *protein TerZ*, *protein TerA*, *protein TerF*, *prohead protease*, and *antirepressor protein* in *E. coli* O160:H7 isolate, which were encoded by *E. coli* O157:H7 (Table S1C). T3SS of *E.coli* O160:H7 was different from other unpathogenic *E.coli* str.k12.substr.MG1655 and pathogenic *E.coli* CFT073 (Table S1C). *E.coli* O160:H7 also encoded type IV secretion system (T4SS) (Table S1D) and other factors, including those for adhesion such as *fim* gene cluster (*fimA*, *fimB*, *fimC*, *fimD*, *fimE*, *fimF*, *fimH*, *fimG*, *fimI*, etc) and *pil* gene cluster (*pilD*, *pilT*), *papC*, and *papD*, and internalization gene such as *csg* etc. (Table S1D). However, other disease-associated factors such as *Afa/Dr* adhesins, *traA* (encoding pilin), and *malX* (marker for pathogenicity-associated island from strain CFT073), which were found in patients (Mansan-Almeida et al., 2013), was not detected in *E.coli* O160:H7 (Table S1D). *E.coli* O160:H7 also had multiple drug-resistant genes such as *oprM*, *emhC*, *ttgC*, *cusC*, *adeK*, *smeF*, *mtrE*, *cmeC*, *gesC*, *acrA*, *mexA*, *adeI*, *smeD*, *mtrC*, and *cmeA* (http://www.ncbi.nlm.nih.gov/bioproject/513139). Taken together, the gene composition of genome in *E.coli* O160:H7 is different from other identified pathogenic and unpathogenic *E. coli*.

We next examine whether *E. coli* O160:H7 may cause pathological responses in gut tissues. Although *E. coli* O160:H7 were infused into *wt* mice, pan-antibiotic–treated *wt* mice and germ-free (GF) mice, no remarkable symptoms of acute gut diseases such as diarrhea, colonic bleeding, and reduced body weight were observed,

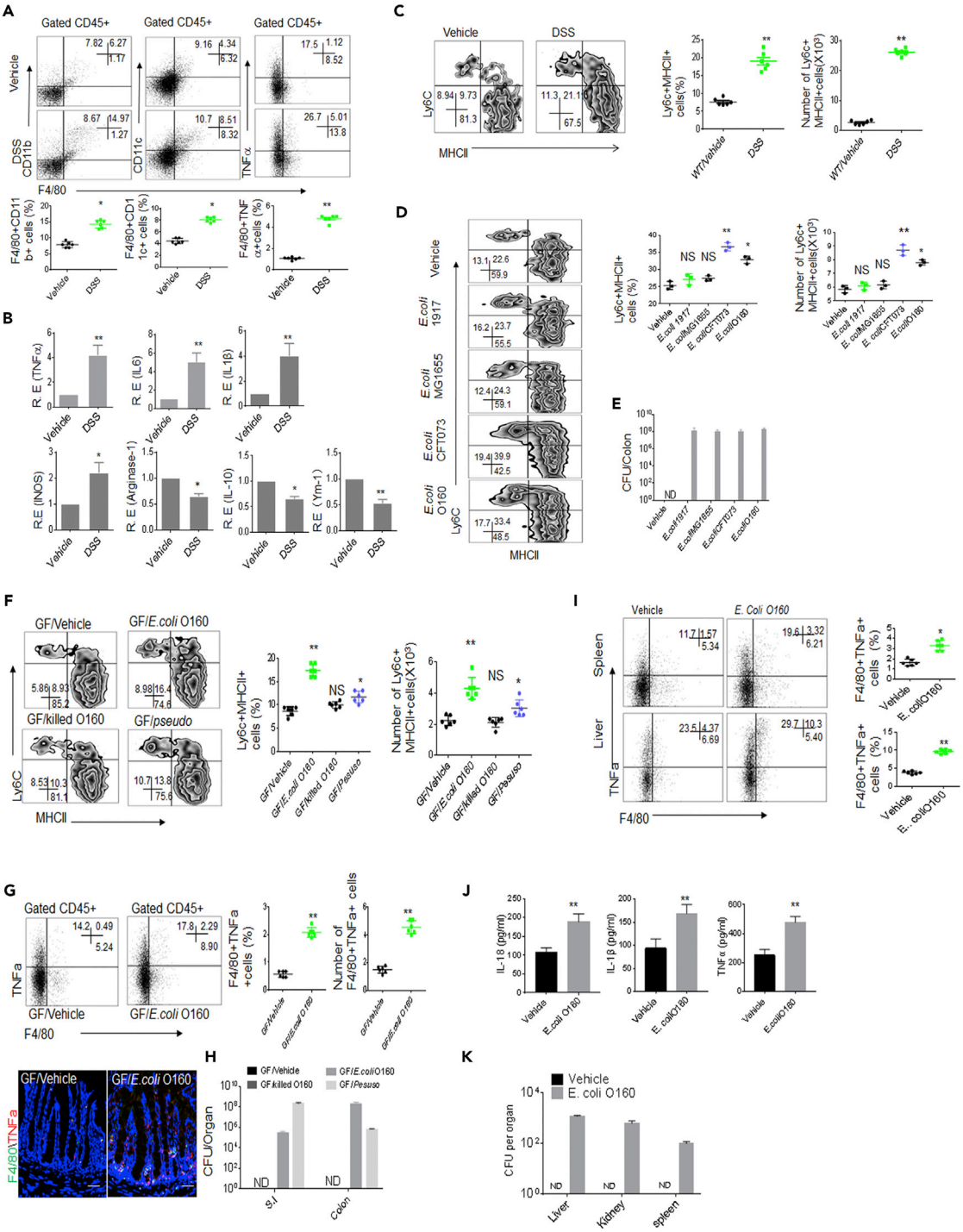

Figure 2. *E. coli* O160:H7 Induces the Accumulation of Inflammatory Macrophages in Colon Tissues

(A) Flow cytometry of F4/80^{+}CD11b^{+}, F4/80^{+}CD11c^{+}, and F4/80^{+}TNFα^{+} cells in DSS-treated and unmolested mice (n = 6).

(B) QRT-PCR of TNFα, IL-6, IL-1β, INOS, arginase-1, and IL-10 in the colon tissues of DSS-treated and unmolested mice (n = 6).

(C) Flow cytometry of MHCII^{+}Ly6C^{+} inflammatory macrophages (CD45^{+}CX3CR1^{+}CD11b^{+}CD103^{-}F4/80^{+} MHCII^{+}Ly6C^{+}) in the colon LP of DSS-treated and unmolested mice (n = 6). % cells and total Ly6c + MHCII+ cell number per colon were analyzed (right).

(D) Flow cytometry of inflammatory macrophages in the colon LP of mice with or without different *E. coli* infusion (n = 3). % cells and total Ly6c + MHCII+ cell number per colon were analyzed (right).

(E) CFU of bacteria in colon tissues of mice infused different *E. coli*.

Figure 2. *Continued*

(F) Flow cytometry of inflammatory macrophages in the colon LP of *E. coli* colonized GF mice (n = 6). GF/pseudo, *pseudomonas*-colonized mice; GF/*E.coli*, *E. coli* O160-colonized mice; GF/killed *E.coli*, dead *E. coli* O160 infused mice. % cells and total Ly6c + MHCII+ cell number per colon were analyzed (right).

(G) Flow cytometry and immunostaining of F4/80$^+$TNFα^+ cells in the colon tissues of GF mice with or without *E. coli* infusion (n = 6). % cells and total F4/80+TNFα+ cell number per colon were analyzed (right). Scale bars = 40 μm.

(H) CFU of bacteria in intestine and colon tissues of *E. coli* infused GF mice.

(I) Flow cytometry of F4/80$^+$TNFα^+ cells in the spleen and liver of mice with or without *E. coli* infusion (n = 6).

(J) ELISA of IL-18, IL-1β, and TNFα in the sera of mice with or without *E. coli* infusion (n = 6).

(K) CFU of bacteria in intestine and colon tissues of mice infused *E. coli.*

Mice in A–C, untreated using pan-antibiotics. Mice in D and I–K, treated using pan-antibiotics for one week before infusing bacteria. For CFU in bacteria infused mice, 10^9 bacteria were orally infused and then CFU were counted after 7 days.

Scale bars = 40 μm in G. ANOVA plus post-Bonferroni analysis in D and F; Two-side Student's *t*-test in A– C, G, I, and J; *p<0.05, **p<0.01, and ***p<0.001; NS, no significance; R. E, relative expression. Data in A–K are represented as mean ± SD. Data in A–K are a representative of two or three independent experiments. See also Figure S3A.

consistent with the genome sequencing data that virulence-related genes are not detected in *E. coli* O160:H7. However, oral administration of *E. coli* O160:H7 promoted sensitivity to DSS-mediated colitis (Figures 1E–lH). This *E.coli* O160:H7 isolate was much more effective than un-dominant *E. coli* IAI39 strain isolated from same mice in promoting sensitivity to DSS-mediated colitis (Figures S2A–S2E). *E. coli* O160:H7was also different from other identified pathogenic *E. coli.* It was weaker than *E. coli* CFT073 but stronger than unpathogenic *E. coli* such as *E. coli* Str. k12.Substr.MG1655 and *E. coli* Nissle 1917 (Figures S2F–S2K). Oral administration of these *E. coli* resulted in high levels of colonization (Figures S2D and S2l)). Notably, *E. coli* O160:H7 isolate and other pathogenic and unpathogenic *E.coli* had a similar ability in inducing TLR4-mediated NF-κB activity (Figure S2L), implying that difference of O160:H7 with other gram-negative *E.coli* in promoting sensitivity to DSS-mediated colitis may not depend on LPS. Taken together, *E.coli* O160:H7 from inflamed colonic tissues promotes sensitivity to DSS-mediated colitis, but it is different from other pathogenic and unpathogenic *E. coli.*

E. coli O160:H7 Induces Inflammatory Macrophages in Gut and Extra-gut Tissues

To elucidate how *E. coli* O160:H7 promotes sensitivity to DSS-mediated colitis, we first examined the composition of gut immune cells in DSS-treated mice. There had remarkably increased F4/80$^+$CD11B$^+$, F4/80$^+$CD11C$^+$, and F4/80$^+$TNFα^+ macrophages in the colon lamina propria (LP) (Figure 2A) and higher levels of inflammatory cytokines in the colonic tissues of mice (Figure 2B), because CD11C and TNFα generally are markers of inflammatory macrophages (Bain et al., 2013), suggesting that there may exist increased inflammatory macrophages in the gut tissues of DSS-treated mice. For gut macrophage subsets, previous multiple studies (Bain et al., 2013; Mortha et al., 2014; Shouval et al., 2014; Tamoutounour et al., 2012) suggest that CX3CR1$^+$CD11b$^+$CD103$^-$F4/80$^+$Ly6C$^+$MHCII$^+$ cells belong to proinflammatory/inflammatory macrophages (P2 stage), whereas CX3CR1$^+$ CD11b$^+$CD103$^-$F4/80$^+$Ly6C$^-$MHCII$^+$cells as anti-inflammatory macrophages (P3 and P4 stage) (Figure S3A). We further investigated the gut macrophage subpopulations using this classification, which was used through this manuscript. The proportion of CD45$^+$CX3CR1$^+$ CD11b$^+$CD103$^-$F4/80$^+$ MHCII$^+$Ly6C$^+$ inflammatory macrophages remarkably increased in the DSS-treated mice (Figure 2C), suggesting that *E. coli* from inflamed colon may induce the inflammatory macrophages. To determine that *E. coli* O160:H7 may induce inflammatory macrophages, we employed *E. coli*-infused mice including broad-spectrum antibiotics AVNM (ampicillin, vancomycin, neomycin, and metronidazole)-treated mice, GF mice, and untreated normal mice. In *E. coli*-infused non-antibiotics *wt* mice, proinflammatory macrophages did not remarkably increase as compared with mice uninfused with *E. coli* (unshown). But, the colonization of *E. coli* O160:H7 isolate could cause significantly increased inflammatory macrophages in AVNM-treated mice and GF mice, in which there existed the dysbiosis of gut microbiota (Figures 2D–2H). There was also significantly increased inflammatory macrophages in extra-gut organs and tissues with higher levels of inflammatory cytokines in peripheral blood in *E. coli*-infused mice, in which *E. coli* were detected (Figures 2I–2K). Thus, although it does not cause remarkable bowel disease symptoms, *E. coli* from the inflamed colon may induce inflammatory macrophages not only in colon tissues but also in extra-gut organs and tissues under the dysbiosis of gut microbiota.

IL-18, IFNγ, IL-12, and IL-22 Are Required in *E. coli*-mediated Gut Inflammatory Macrophages

We next want to understand how *E. coli* O160:H7 isolate induces inflammatory macrophages in colon tissues. Intestinal mononuclear phagocytes do not or only slightly produce inflammatory responses when stimulated with TLR (toll-like receptor) ligands, commensal, or pathogenic bacteria (Franchi et al., 2012). However, IFNγ may promote the generation of inflammatory macrophages (Hu and Ivashkiv, 2009).

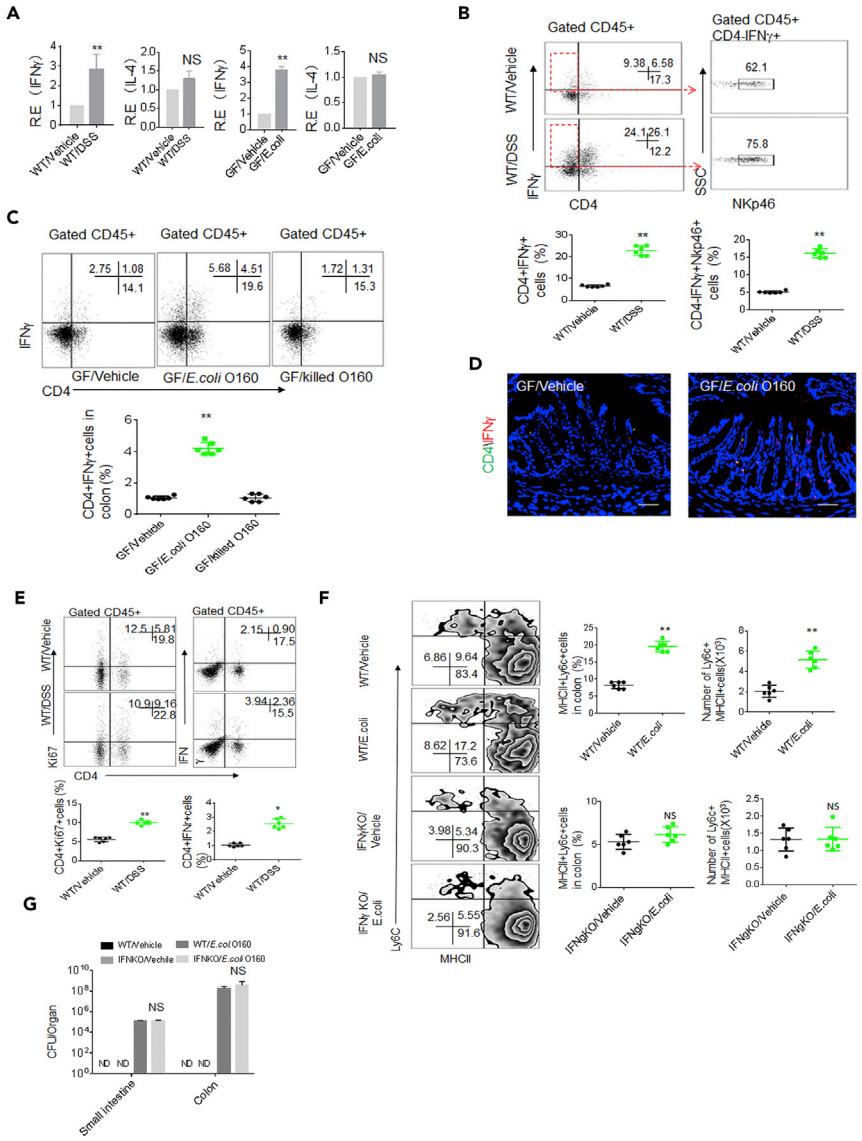

Figure 3. *E. coli* O160:H7-mediated Inflammatory Macrophages Depends on IFN in Gut Tissues

(A) QRT-PCR of IFNγ and IL4 in the colon tissues of DSS-treated (WT/DSS) and unmolested mice (WT/Vehicle) or GF mice with (GF/*E. coli*) or without *E.coli* (Vehicle) infused GF (n = 6).

(B) Flow cytometry of $CD4^+IFN\gamma^+$ and $CD4^-NKp46^+$cells in colon tissues of DSS-treated (WT/DSS) and unmolested (WT/Vehicle) mice (n = 6).

(C) Flow cytometry of $CD45^+CD4^+IFN\gamma^+$ cells in the colon LP of *E. coli* infused GF mice (n = 6). GF/killed E.coli, dead *E.coli* infused GF mice.

(D) Immunostaining of $CD4^+IFN\gamma^+$ cells in colon tissues of *E. coli* infused GF mice (n = 6).

(E) Flow cytometry of $CD4^+Ki67^+$ and $CD4^+IFN\gamma^+$ cells in the payer's patch of DSS-treated and un-treated mice (n = 6).

(F) Flow cytometry of inflammatory macrophages in the colon LP of IFNγ−/− mice infused (*E. coli*) or uninfused (Vehicle) *E.coli* O160:H7 (n = 6). % cells and total Ly6c + MHCII+ cell number per colon were analyzed (right).

(G) CFU in intestine and colon tissues. GF mice were infused with 10^9*E. coli* and then CFU were counted after 7 days (n = 6).

Scale bars = 40 μm in D. Two-side student's *t*-test in A–C and E–G; *p<0.05, **p<0.01, and ***p<0.001; NS, no significance; R. E, relative expression. Data in A, B, C, E, F, and G are represented as mean ± SD. Data are a representative of two or three independent experiments. See also Figure S3.

Remarkably increased IFNγ was detected not only in DSS-mediated colitis but also in *E.coli* O160:H7 colonized colon tissues as compared with their control mice, whereas other anti-inflammatory cytokines such as IL-4 did not significantly change (Figure 3A). There also existed a drastic expansion of interferon

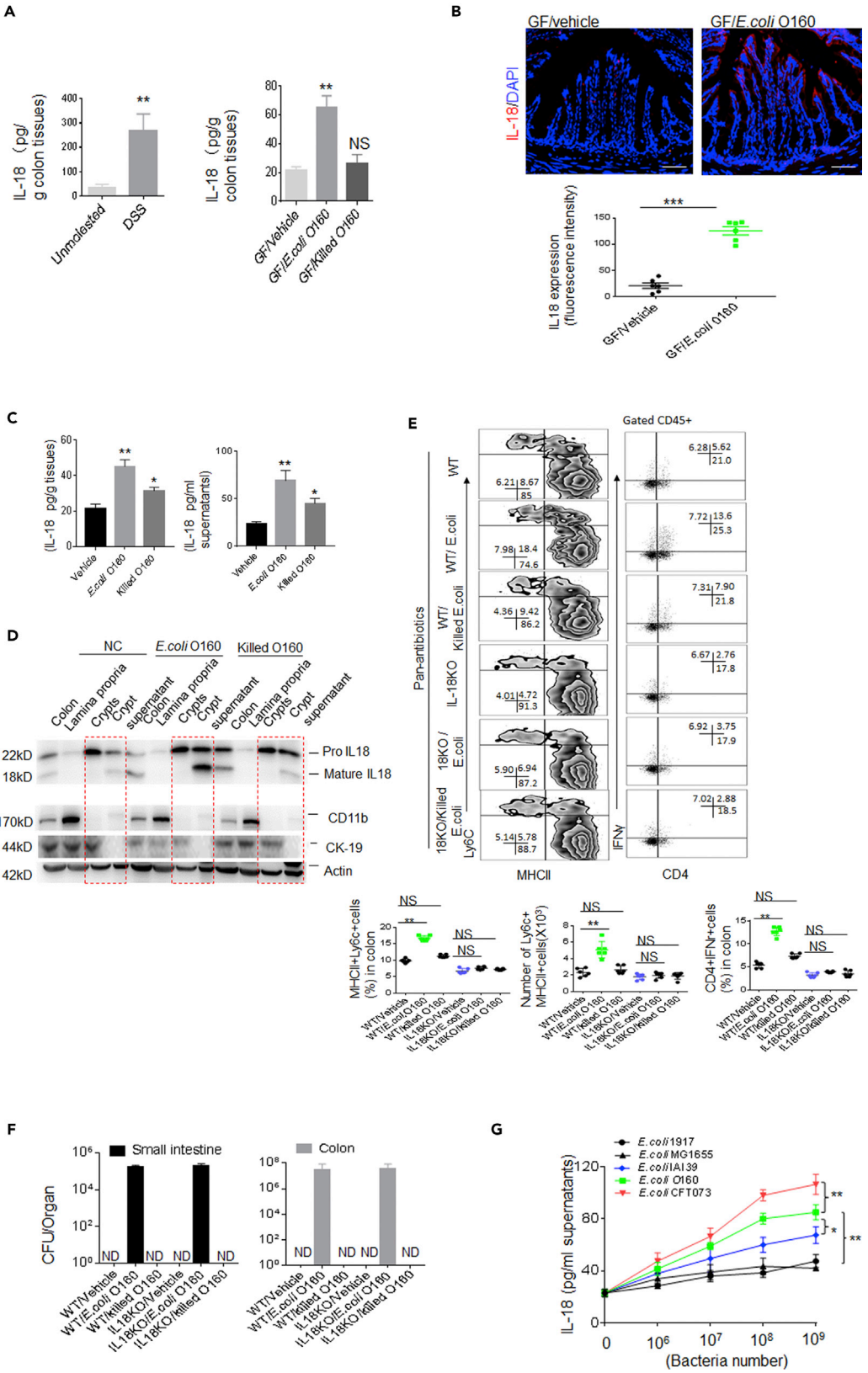
A
IL-18 (pg/g colon tissues)
Unmolested
DSS
IL-18 (pg/g colon tissues)
GF/Vehicle
GF/E.coli O160
GF/Killed O160
NS
B
GF/vehicle
GF/E.coli O160
IL-18/DAPI
IL18 expression (fluorescence intensity)
GF/Vehicle
GF/E.coli O160
C
(IL-18 pg/g tissues)
(IL-18 pg/ml supernatants)
Vehicle
E.coli O160
Killed O160
D
NC
E.coli O160
Killed O160
Colon
Lamina propria
Crypts
Crypt
supernatant
22kD
18kD
Pro IL18
Mature IL18
170kD
CD11b
44kD
CK-19
42kD
Actin
E
Gated CD45+
Pan-antibiotics
WT
WT/ E.coli
WT/ Killed E.coli
IL-18KO
18KO / E.coli
18KO/Killed E.coli
Ly6C
MHCII
CD4
IFNγ
MHCII+Ly6c+cells (%) in colon
Number of Ly6c+ MHCII+cells(X10³)
CD4+IFN+cells (%) in colon
WT/Vehicle
WT/E.coli O160
WT/killed O160
IL-18KO/Vehicle
IL-18KO/E.coli O160
IL-18KO/killed O160
F
CFU/Organ
Small intestine
Colon
ND
G
E.coli 1917
E.coli MG1655
E.coli IAI39
E.coli O160
E.coli CFT073
IL-18 (pg/ml supernatants)
(Bacteria number)

Figure 4. *E. coli* O160:H7-mediated Inflammatory Macrophages depends on the Gut Epithelial Cells Derived IL-18

(A) ELISA of IL-18 in the colon tissues of mice with (DSS) or without DSS or GF mice infused with or without *E. coli* (n = 6, male). GF/killed E.coli, heat-killed *E.coli* infused mice.

(B) Immuno-staining of IL-18 in colon tissues of GF mice infused with *E. coli* (n = 6). GF/vehicle, only vehicle.

(C) ELISA of IL-18 in the supernatants of gut epithelial cells after exposed to *E. coli* O160:H7 or heat-killed *E. coli* O160:H7 (Killed E.coli) for 1 h.

(D) Immunoblotting of IL-18 in colon tissues, colon lamina propria, crypts, and crypt supernatants after exposed to *E. coli* O160:H7 or heat-killed *E. coli*O160:H7 (killed E.coli). Cytokeratin 19 (CK19) is a marker of epithelial cells; CD11b is a marker of macrophages; actin is a loading control.

(E) Flow cytometry of inflammatory macrophages and CD4+IFNγ+ cells in the colon LP of *wt* and IL-18−/− mice colonized *E. coli* O160:H7 (n = 6). % cells and total Ly6c + MHCII+ cell number per colon were analyzed (Lower).

(F) CFU/organ tissues in *E. coli* O160:H7 oral infused mice, which were treated with pan-antibiotics (AVNM) for 7 days.

(G) ELISA of IL-18 in the colon tissues of *wt* mice in response to different kinds of bacteria. *E. coli* 1917; O160, *E.coli* O160:H7, G1655, *E. coli* G1655; CFT073, E.coli CFT073.

Scale bars = 40 μm in B. Two-side Student's *t*-test in A (left), B and E; ANOVA plus post-Bonferroni analysis in A (right) and C; analysis of variance test in G. *p<0.05, **p<0.01, and ***p<0.001; NS, no significance; R. E, relative expression. Data in A–C and E–G are represented as mean ± SD. Data for all panels are a representative from two to three experiments.

γ (IFNγ)-producing $CD4^+$ T helper cells (Th1) cells ($CD4^+IFN\gamma^+$Th1 cells) and $NKp46^+$ $IFN\gamma^+$ cells in the LP tissues of DSS-mediated colitis and *E. coli* O160:H7-colonized mice (Figures 3B–3D). Because $Ly6C^+$ monocytes can give rise to a CCR7-expressing $CX3CR1^{int}$ $Ly6C^{lo}$ cell population capable of migrating into lymph node and priming T cells toward Th1 under inflammatory conditions, increased $CD4^+Ki67^+$ T and $CD4^+IFN\gamma^+$cells were also detected in the PP (Figure 3E). The colonization of *E. coli* O160:H7 in IFNγ−/− mice did not cause accumulated inflammatory macrophages in the colonic LP (Figures 3F and 3G). Thus, our results demonstrate that gut IFN-γ plays a critical role in *E. coli* O160:H7-mediated inflammatory macrophages in colonic tissues.

IL-18 has been shown to play an important role in the induction of IFNγ production, increasing NK cell activity and T cell proliferation (Nielsen et al., 2016). There also are substantial evidences for the expression and secretion of IL-18 by the intestinal epithelium. Thus, we detected whether the accumulated IFNγ producing cells were related to IL-18 in the gut epithelial cells. Indeed, the increased IL-18 was detected in the gut epithelial cells of *E. coli* O160:H7-colonized mice and also DSS-induced colitic tissues (Figures 4A and 4B). More mature IL-18 was also detected in crypt supernatants after *in vitro* stimulation by *E.coli* O160:H7 (Figures 4C and 4D). The colonization of *E. coli* O160:H7 in IL-18 −/− mice did not cause the accumulation of inflammatory macrophages in the colonic LP (Figures 4E and 4F). In addition, both IL-22 and IL-12 also induce IL-18 expression in epithelial cells during intestinal infection (Munoz et al., 2015). Higher levels of IL-22 and IL-12 were detected in the gut tissues of *E. coli*-colonized mice (Figure S3B). IL-22 and IL-12 blocking reduced the expression of IL-18 and inhibited the accumulation of inflammatory macrophages (Figure S3C). Finally, we also compared the ability of *E. coli* O160:H7 with that of other *E. coli* strains in inducing mature IL-18. *E. coli* O160:H7 induced more IL-18 production than other unpathogenic bacteria but weaker as compared with pathogenic *E. coli* CFT073 in colon epithelial cells (Figure 4G). Taken together, gut epithelial cells derived IL-18 is involved in the increased inflammatory macrophages.

PCKδ, NLRC4, caspase8, and caspase1/11 Are Required for *E. coli* O160:H7-Induced IL-18

Next question is how *E. coli* O160:H7 induces the expression of IL-18 in gut epithelial cells. The inactive 24 kDa precursor pro-IL-18 is constitutively expressed by gut epithelial cells and primed for release upon inflammasome activation. Gut epithelial cells have revealed an expression of an array of inflammasome components including NAIP, NLRP (NOD-like receptor protein) 1, NLRC4, NLRP6, AIM2, caspase1, caspase4/5 (human)/caspase11 (mouse), caspase8, ASC, and NLRP6/3 (von Moltke et al., 2013). Cytosolic pattern recognition receptors (PRRs) are often associated with the use of pore-forming toxins or injection of effecter molecules through specialized secretion systems of gram-negative bacteria (von Moltke et al., 2013), which are encoded by *E. coli* O160:H7. Because inner rod protein of type three secretion systems (TTSS) and functional flagellin (FliC) of gram-negative bacteria-mediated production of mature IL-18 mainly is through NLRC4/caspase1 signal pathway (Miao et al., 2010), we investigated the effects of NLRC4 and caspase1 on *E.coli* O160:H7-mediated mature IL-18. We found that NLRC4 and caspase1/11 was involved in *E. coli* O160:H7-mediated IL-18 release (Figures 5A–5C and S4A–S4C). More recent studies have revealed a requirement for caspase8 in activating caspase1 within the inflammasome complex (Man and Kanneganti, 2016). The caspase8 specific inhibitor did also affect *E.coli* O160:H7-mediated mature IL-18 (Figures 5D and 5E). The phosphorylation of NLRC4, which is activated by PKCδ in *Salmonella* infection, was necessary in macrophages (Qu et al., 2012). PKCδ inhibitor also impaired *E.coli* O160:H7-mediated mature IL-18 in gut epithelial cells (Figures 5D and 5E). Finally, immunoprecipitation further identified

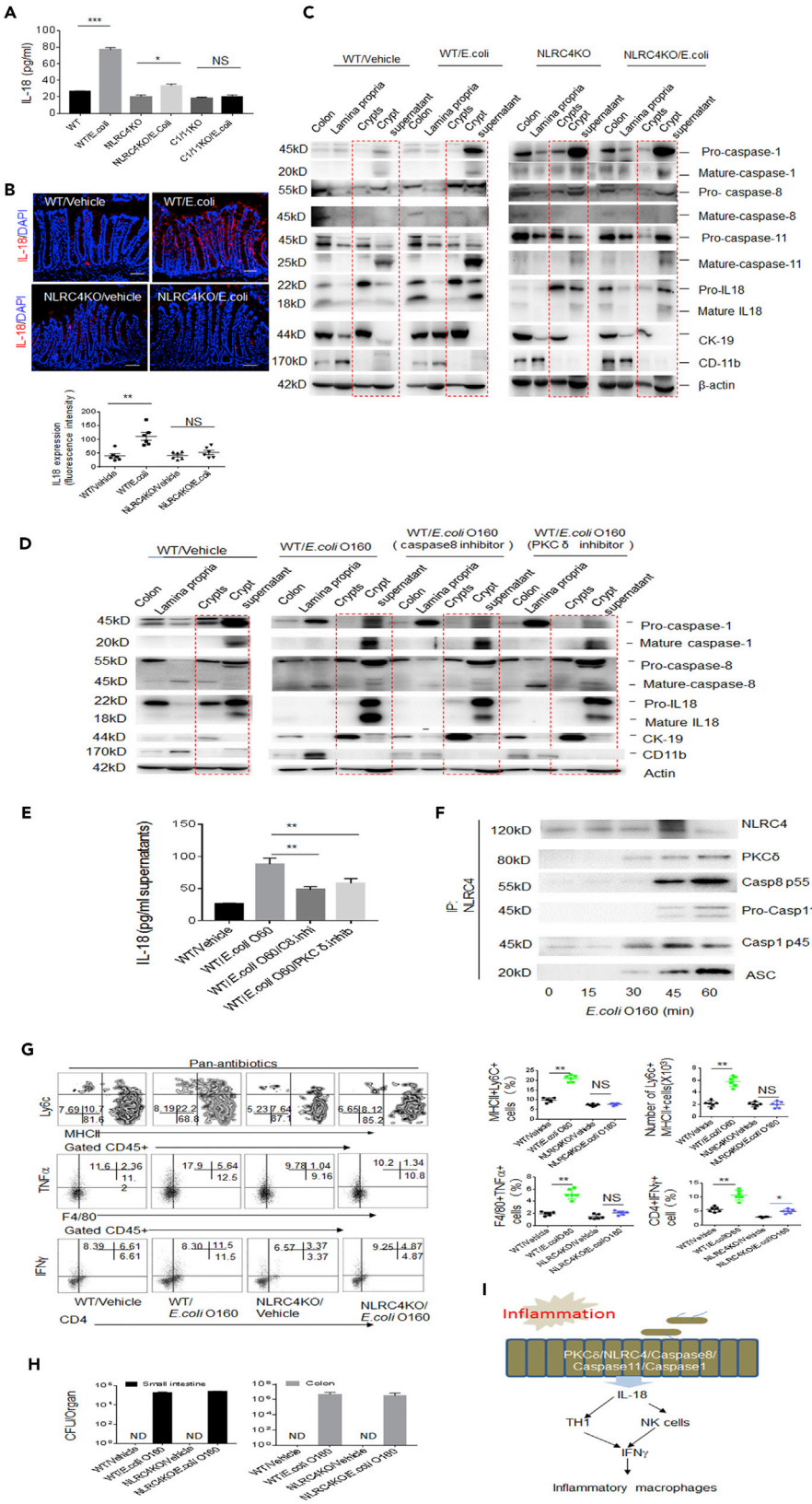
A
IL-18 (pg/ml)
WT
WT/E.coli
NLRC4KO
NLRC4KO/E.coli
C1f1KO
C1f1KO/E.coli
B
WT/Vehicle
WT/E.coli
NLRC4KO/vehicle
NLRC4KO/E.coli
IL-18/DAPI
IL18 expression (fluorescence intensity)
C
WT/Vehicle
WT/E.coli
NLRC4KO
NLRC4KO/E.coli
Colon
Lamina propria
Crypts
Crypt supernatant
Pro-caspase-1
Mature-caspase-1
Pro- caspase-8
Mature-caspase-8
Pro-caspase-11
Mature-caspase-11
Pro-IL18
Mature IL18
CK-19
CD-11b
β-actin
D
WT/Vehicle
WT/E.coli O160
WT/E.coli O160 (caspase8 inhibitor)
WT/E.coli O160 (PKC δ inhibitor)
Pro-caspase-1
Mature caspase-1
Pro-caspase-8
Mature-caspase-8
Pro-IL18
Mature IL18
CK-19
CD11b
Actin
E
IL-18 (pg/ml supernatants)
WT/Vehicle
WT/E.coli O60
WT/E.coli O60/Cβ.inhi
WT/E.coli O60/PKC δ.inhib
F
IP: NLRC4
NLRC4
PKCδ
Casp8 p55
Pro-Casp11
Casp1 p45
ASC
E.coli O160 (min)
G
Pan-antibiotics
Ly6c
MHCII
Gated CD45+
TNFα
F4/80
IFNγ
CD4
WT/Vehicle
WT/ E.coli O160
NLRC4KO/ Vehicle
NLRC4KO/ E.coli O160
MHCII+Ly6C+ cells (%)
Number of Ly6c+ MHCII+cells(X10⁵)
F4/80+TNFα+ cells (%)
CD4+IFNγ+ cell (%)
H
CFU/Organ
Small intestine
Colon
ND
I
Inflammation
PKCδ/NLRC4/Caspase8/ Caspase11/Caspase1
IL-18
TH1
NK cells
IFNγ
Inflammatory macrophages

Figure 5. *E. coli* O160:H7 Induces IL-18 Through PCKδ/NLRC4/Caspase8/CASPASE11/1 Complexes in Colon Epithelial Cells

(A) ELISA of IL-18 in the supernatants of colon epithelial cells of wt, NLRC4−/−, or caspase1/11 −/− mice in response to *E. coli* O160:H7.

(B) Immunostaining of IL-18 in colon epithelial cells of wt, NLRC4−/−, and caspase1/11 −/− mice after infusing *E. coli* O160:H7 (n = 6). Scale bars = 40 μm.

(C) Immunoblotting in lamina propria, crypts, and crypt supernatants of colon tissues in wt and NLRC4 −/− mice after exposed to *E. coli* O160:H7 for 1 h.

(D) Immunoblotting in colon tissues, lamina propria, crypts, and crypt supernatants of wt mice after exposed to *E. coli* for 1 h with or without caspase8 and PKC inhibitors.

(E) ELISA of IL-18 in the supernatants of colon epithelial cells of wt mice after exposed to *E. coli* for 1 h with or without caspase8 and PKC inhibitors.

(F) Immunoprecipitation of NLRC4 after cross-linking in the colon epithelial cells of wt after exposed to *E. coli* O160:H7.

(G) Flow cytometry of inflammatory macrophages and $CD4^+IFN\gamma^+$ cells in the LP of colon tissues of NLRC4 −/− mice infused *E. coli* O160:H7 (n = 6).

(H) CFU/colon tissues in *E. coli* O160:H7 orally infused mice, which were treated with pan-antibiotics for 7 days.

(I) Model for *E. coli* O160:H7-mediated inflammatory macrophages. *E. coli* O160:H7 induces mature IL-18 in colon epithelial cells through PKCδ/NLRC4/Caspase8/caspase11/caspase1 complexes.

Scale bars = 40 μm in B. Two-side student's *t*-test in A, E, and G; *p<0.05, **p<0.01, and ***p<0.001; NS, no significance; R. E, relative expression. Data in A, E, G, and H are represented as mean ± SD; data in B are represented as mean ± SEM; data in all panels are a representative of two or three independent experiments. See also Figures S4 and S5.

bioactive PCKδ, caspase1, caspase8, and ASC molecules being bound by NLRC4 in colon epithelial cells (Figure 5F), which are shown in macrophages infected with *S. Typhimurium* (Man et al., 2014). Interestingly, NLRC4 complexes also included caspase11 in colon epithelial cells (Figure 5F). It was also found that the noncanonical inflammasome also activates caspase11 in response to many gram-negative bacteria (Kayagaki et al., 2011). Critically, the colonization of *E. coli* O160:H7 in NLRC4 −/− or caspase1/11 −/− mice did not cause accumulated inflammatory macrophages in colonic LP (Figures 5G, 5H, and S4D). In addition, caspase11 and NLRC4 inflammasome activation in gut epithelial cells may lead to a lytic cell death, resembling pyroptosis (Rauch et al., 2017). There had increased PI^+ cells (pyroptosis cells) in *E.coli* O160:H7 colonized GF mice, indicating that this strain of *E. coli* also induced pyroptosis of gut epithelial cells (Figure S5). As a result, this may promote the penetration of *E. coli* into extra-gut tissues. Taken together, we demonstrate that *E. coli* O160:H7 may induce the production of mature IL-18 through an inflammasome complex consisted of PKCδ, NLRC4, caspase8, and caspase1/11 in gut epithelial cells (Figure 5I).

E. coli O160:H7 Directly Induces IL-18 and IL-1β in Macrophages

We also observed effect(s) of *E. coli* O160:H7 isolate on the macrophages. *E. coli* O160:H7 directly activated macrophages to induce IL-1β and IL-18 *in vitro* (Figures 6A–6C). Furthermore, *E. coli* O160:H7-mediated production of IL-18 and IL-1β was also dependent on signal pathway consisted of PCKδ, NLRC4, caspase8, and caspase1/11 signal pathway in macrophages (Figures 6A–6E). Intravenous injection of *E. coli* O160:H7 into normal *wt* mice caused rapidly increased IL-18 and IL-1β in peripheral blood and accumulation of inflammatory macrophages in spleen and liver (Figures 6F and 6G). NLRC4−/− and caspase1/11 −/− and IL-18−/− impaired this ability of *E. coli* O160:H7 to induce the production of IL-1β and IL-18 (Figures 6F and 6G). These bacteria could effectively localize in these tissues and organs (Figure 6H). Meanwhile, we also found that *E. coli* O160:H7 was more effective in inducing mature IL-18 or IL-1β than other unpathogentic *E. coli* (Figures 6I and 6J). Thus, *E. coli* O160:H7 also directly induce production of IL-18 and IL-1β in macrophages through activating inflammasome complexes including PCKδ, NLRC4, caspase8, and caspase11/1.

E. coli O55: HNT from Patients has Similar Function with *E. coli* O160:H7

We also investigate a dominant *E. coli* O55: HNT strain from colitic tissues of patients with inflammatory bowel disease. The increased *E. coli* could be detected in colitic tissues of patients with inflammatory bowel disease (Figures 7A and 7B), consistent with other data (Winter and Baumler, 2014). We found that the isolated *E. coli* O55: HNT from colitic tissues of patients with inflammatory bowel disease (Table S1E) had a similar function with mouse *E. coli* O160:H7 isolate. This strain *E. coli* O55: HNT also promoted sensitivity to DSS-mediated colitis (Figures 7C–7F) and induced inflammatory macrophages (Figure 7G). *In vivo* intravenously administration also caused increased inflammatory macrophages in the colonized tissues and organs (Figures 7H and 7I).

We finally compared the effects of *E. coli* O55: HNT and *E. coli* O160:H7 strain with other identified pathogenic and unpathogenic *E. coli* on mortality and morbidity after oral administration and *in vivo*

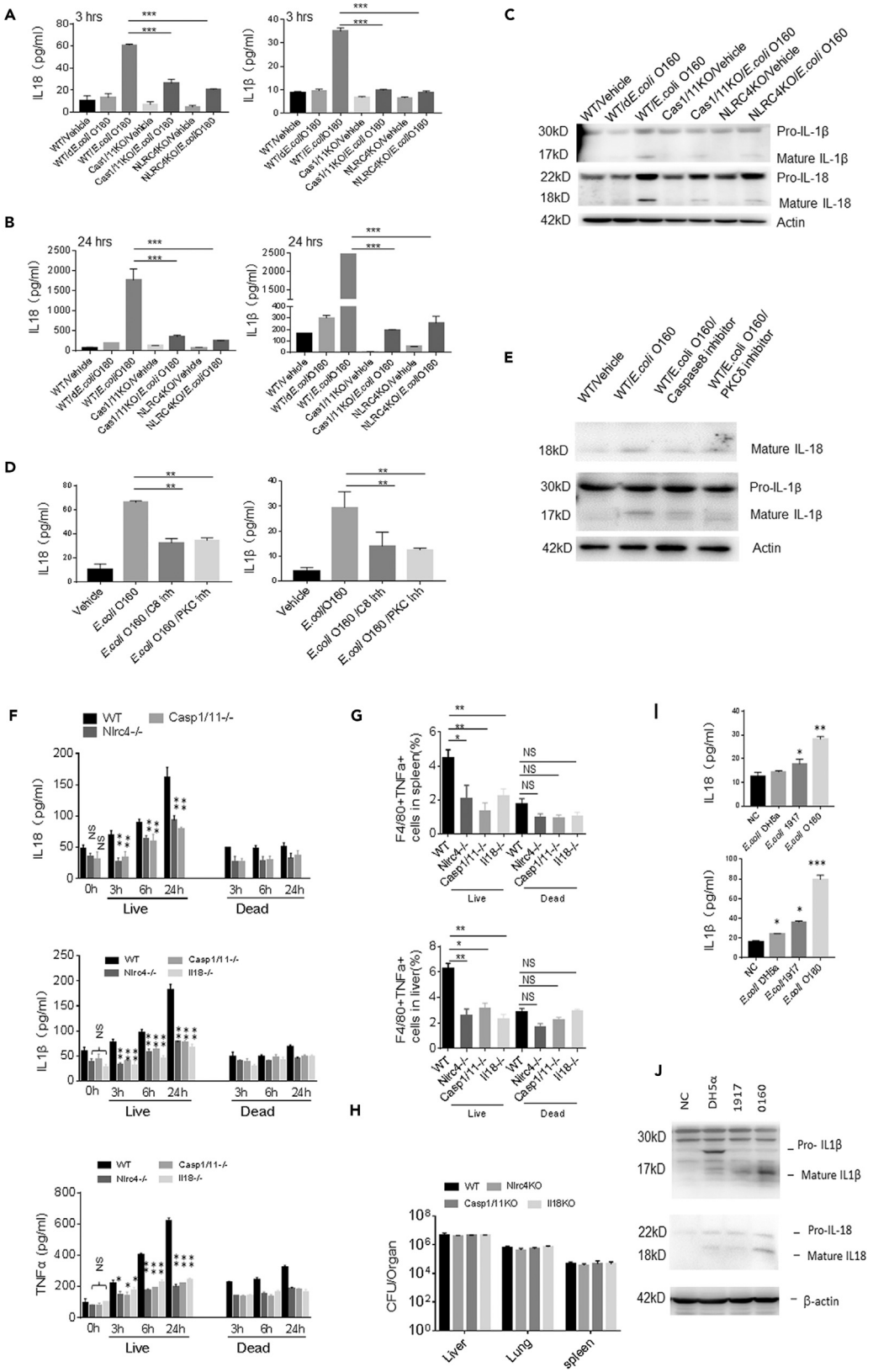
A
3 hrs
IL18 (pg/ml)
IL1β (pg/ml)
WT/Vehicle
WT/dE.coli O160
WT/E.coli O160
Cas1/11KO/Vehicle
Cas1/11KO/E.coli O160
NLRC4KO/Vehicle
NLRC4KO/E.coli O160
B
24 hrs
C
30kD
17kD
22kD
18kD
42kD
Pro-IL-1β
Mature IL-1β
Pro-IL-18
Mature IL-18
Actin
D
Vehicle
E.coli O160
E.coli O160 /C8 inh
E.coli O160 /PKC inh
E
WT/E.coli O160/ Caspase8 inhibitor
WT/E.coli O160/ PKCδ inhibitor
F
WT
Casp1/11-/-
Nlrc4-/-
Il18-/-
TNFα (pg/ml)
0h
3h
6h
24h
Live
Dead
G
F4/80+TNFa+ cells in spleen(%)
F4/80+TNFa+ cells in liver(%)
NS
H
Nlrc4KO
Casp1/11KO
Il18KO
CFU/Organ
Liver
Lung
spleen
I
NC
DH5α
1917
J
Pro- IL1β
Mature IL1β
Pro-IL-18
Mature IL18
β-actin

Figure 6. *E. coli* O160:H7 Directly Stimulates Macrophage to Produce IL-18 and IL-1 β

(A and B) ELISA of IL-18 and IL-1β in the supernatants of macrophages after exposed to *E. coli* O160:H7 at 3 h (A) and 24 h (B).

(C) Immunoblotting of pro-IL-1β, mature IL-1β, pro-caspase18, and mature IL-18 in the macrophages after exposed to *E. coli* for 1 h.

(D) IL-18 ELISA and immunoblotting after exposed to *E. coli* O160:H7 for 3 h in the presence of caspase8 and PKCδ inhibitor.

(E) Immunoblotting after exposed to *E. coli* O160:H7 with or without caspase8 and PKCδ inhibitors for 3 h.

(F) ELISA of IL-18, IL-1β, and TNFα in the peripheral blood of wt, NLRC4−/−, and caspase1/11−/− mice after injecting *E. coli* O160:H7 or heat-killed *E. coli* in tail vein at the indicated time (n = 6).

(G) Flow cytometry of $F4/80^{+}TNF\alpha^{+}$ macrophages in spleen and liver of wt, NLRC4−/−, and caspase1/11 −/− mice after injecting *E. coli* or heat-killed *E. coli* in tail vein (n = 6).

(H) CFU of *E. coli* in the spleen, liver, and lung of wt, NLRC4−/−, and caspase1/11 −/− mice after injecting *E. coli* in tail vein.

(I) ELISA of IL-18 and IL-1β in the macrophages after exposed to DH5α, *E.coli* 1917, or *E.coli* O160:H7 for 3 h.

(J) Immunoblotting of in the macrophages after exposed to DH5α, *E.coli* nissle.1917 (1917); *E. coli* O160:H7 (O160).

ANOVA plus post-Bonferroni analysis in A, B, D, and F–I. *p<0.05, **p<0.01, and ***p<0.001; NS, no significance; R. E, relative expression. Data in A, B, D, F–I are represented as mean ± SD. Data are a representative of three independent experiments.

intravenous administration. Notably, *E. coli* O55: HNT was similar to *E. coli* O160:H7 strain but not to pathogenic *E. coli* such as *E. coli* CFT073 in mortality and morbidity. Although oral administration of *E. coli* CFT073 caused remarkable symptom of acute gut diseases, the mice administrated with *E. coli* O55: HNT did not exhibit detectable symptom (Figures S6A and S6B). Colon inflammation was observed only in *E. coli* CFT073 but not in *E. coli* O55: HNT or *E. coli* O160:H7 infused *wt* mice (Figures S6A and S6B). Although oral administration of *E. coli* in pan-antibiotics-treated mice or GF mice, *E. coli* O55: HNT or *E. coli* O160:H7 could cause symptom of acute gut diseases and colon inflammation but much slighter than *E. coli* CFT073 (Figures S6C and S6D). In *in vivo* intravenous administration mice, *E. coli O55*: HNT and *E. coli O160*:H7 could cause disease symptoms. However, these symptoms were remarkably slighter than pathogenic bacteria *E. coli* CFT073 (Figures S6E and S6F) although it is significantly severe than unpathogenic bacteria *E. coli* MG1655 (Figures S6E and S6F). Intravenous injection also exhibited tissue colonization pattern (Figure S6G). Taken together, there are remarkable differences in mortality and morbidity between *E. coli* O55:HNT and *E. coli* O160:H7 isolated from colitic tissues and other pathogenic *E. coli*.

DISCUSSION

In this study, we found that a high abundance of commensal *E. coli* in inflamed colonic tissues are different from other unpathogenic commensal *E. coli* and also pathogenic *E. coli* in their genome, especially T3SS and virulent factors. These *E. coli* may induce inflammatory macrophages in the colon tissues and extra-gut tissues but not acute infection diseases. They stimulate gut epithelial cells to produce IL-18 through inflammasome complexes that consisted of PKC δ, NLRC4, caspase8, and caspase1/11. IL-18 derived from gut epithelial cells induces Th1- and $NKp46^{+}$ IFNγ-producing cells, which are necessary for the generation of inflammatory macrophages. Meanwhile, higher levels of IL-12 and IL-22 in the colon tissues are also involved in *E. coli*-mediated inflammatory macrophages. The isolated *E. coli* not only induce gut inflammatory macrophages but also directly activate extra-gut macrophages to produce proinflammatory cytokines. There also have increased pyroptosis cells in the *E. coli*-colonized mice, which may potentially promote microbial translocation into the distal tissues and/or organs. These data disclose a new mechanism for how colitis associated gut microbiota to cause inflammatory macrophages in the gut and extra-gut tissues and organs. Since inflammatory macrophages are related to multiple systemic diseases such as inflammatory bowel disease (IBD), obesity, atherosclerosis, carcinogenesis, etc (Blander et al., 2017), our results imply that a high abundance of commensal *E. coli* in inflamed gut may play a role in the occurrence and development of these diseases. Thus, our data suggest a possible mechanism for the occurrence and development of chronic inflammation diseases, which are related to inflammatory macrophages.

Generally, gram-negative bacteria may activate inflammasomes through LPS-caspase11/1 and/or flagellin-NLRC4-caspase1 pathway to induce the production of mature IL-18 in macrophages and epithelial cells. However, several studies have exhibited difference of gram-negative bacteria in their ability to induce production of inflammatory cytokines. Pathogenic *E. coli* but not commensal bacteria can elicit substantial amounts of mature IL-1β by the NLRC4 pathway (Franchi et al., 2012; Lightfield et al., 2008). *E. coli* Nissle 1917 and commensal *E. coli* K12 also differentially affect the inflammasome in intestinal epithelial cells (Becker et al., 2014). We here also found that there exists a remarkable difference between inflamed colonic tissues derived *E. coli* and other unpathogenic and pathogenic *E. coli* in inducing inflammatory macrophages. Recently, *E. coli* strains from antibiotic-treated mice may cause lethal inflammasome activation through NLRC4 (Ayres et al., 2012), whereas another strain E. coli, which also activate NLRC4, may protect

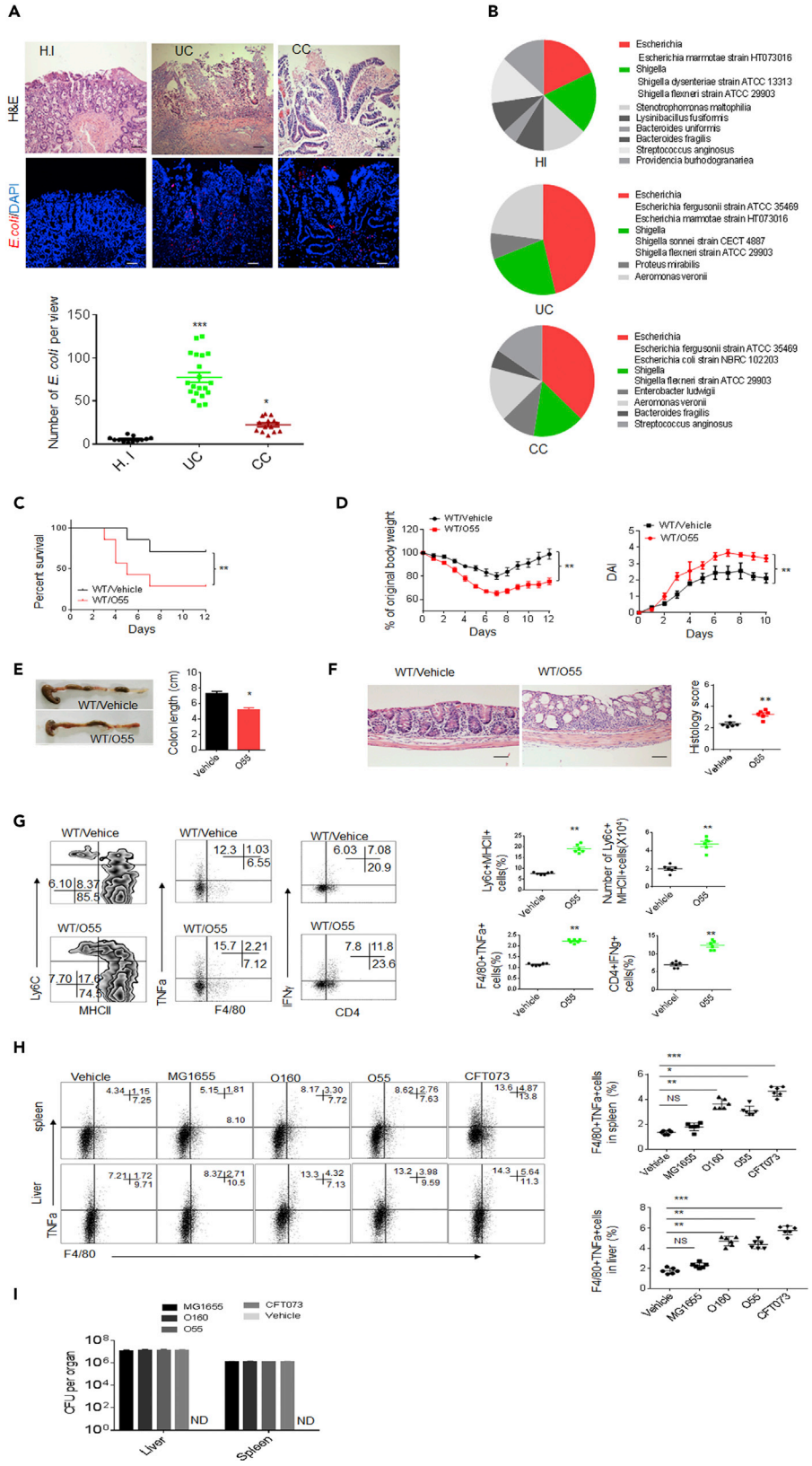
A
H.I
UC
CC
H&E
E.coli/DAPI
Number of E. coli per view
150
100
50
0
***
*
H. I
UC
CC
B
Escherichia
Escherichia marmotae strain HT073016
Shigella
Shigella dysenteriae strain ATCC 13313
Shigella flexneri strain ATCC 29903
Stenotrophomonas maltophilia
Lysinibacillus fusiformis
Bacteroides uniformis
Bacteroides fragilis
Streptococcus anginosus
Providencia buhodogranariea
HI
Escherichia
Escherichia fergusonii strain ATCC 35469
Escherichia marmotae strain HT073016
Shigella
Shigella sonnei strain CECT 4887
Shigella flexneri strain ATCC 29903
Proteus mirabilis
Aeromonas veronii
UC
Escherichia
Escherichia fergusonii strain ATCC 35469
Escherichia coli strain NBRC 102203
Shigella
Shigella flexneri strain ATCC 29903
Enterobacter ludwigii
Aeromonas veronii
Bacteroides fragilis
Streptococcus anginosus
CC
C
Percent survival
100
50
0
WT/Vehicle
WT/O55
**
0 2 4 6 8 10 12
Days
D
% of original body weight
120
100
80
60
WT/Vehicle
WT/O55
**
0 2 4 6 8 10 12
Days
DAI
5
4
3
2
1
0
WT/Vehicle
WT/O55
**
0 2 4 6 8 10
Days
E
WT/Vehicle
WT/O55
Colon length (cm)
10
8
6
4
2
0
*
Vehicle
O55
F
WT/Vehicle
WT/O55
Histology score
6
4
2
0
**
Vehicle
O55
G
WT/Vehicle
WT/O55
6.10 8.37 85.5
7.70 17.6 74.5
Ly6C
MHCII
12.3 1.03 6.55
15.7 2.21 7.12
TNFa
F4/80
6.03 7.08 20.9
7.8 11.8 23.6
IFNγ
CD4
Ly6c+MHCII+ cells(%)
Number of Ly6c+ MHCII+cells(X10⁴)
F4/80+TNFa+ cells(%)
CD4+IFNg+ cells(%)
Vehicle
O55
H
Vehicle
MG1655
O160
O55
CFT073
spleen
Liver
TNFa
F4/80
4.34 1.15 7.25
5.15 1.81 8.10
8.17 3.30 7.72
8.62 2.76 7.63
13.6 4.87 13.8
7.21 1.72 9.71
8.37 2.71 10.5
13.3 4.32 7.13
13.2 3.98 9.59
14.3 5.64 11.3
F4/80+TNFa+cells in spleen (%)
F4/80+TNFa+cells in liver (%)
***
*
**
NS
Vehicle
MG1655
O160
O55
CFT073
I
MG1655
O160
O55
CFT073
Vehicle
CFU per organ
10⁸
10⁶
10⁴
10²
10⁰
ND
Liver
Spleen

Figure 7. Isolated *E. coli* 055:HNT from Colitic Tissues of Patients with Ulcerative Colitic Indirectly and Directly Induce Proinflammatory Macrophages

(A) H&E (Upper) and FISH (Lower) of healthy individuals and patients with ulcerative colitic (UC) and colon cancer (CC). Scale bars = 40 μm.

(B) Proportion of *E.coli* in colon tissues of healthy individuals (n = 17) and patients with ulcerative colitis (UC, n = 20) and colitic cancer (CC, n = 15), which were grown in LP plates.

(C and D) Survival rate (C), body weight, and disease index (D) were monitored in mice infused by *E. coli* 055:HNT after the start of DSS (n = 12).

(E) Length of colon were monitored in mice infused by *E. coli* 055:HNT after DSS treatment.

(F) H&E staining and histological scores of colon tissues in mice infused by *E. coli* 055: HNT after DSS treatment. Scale bars = 40 μm.

(G) Flow cytometry of inflammatory macrophages, $F4/80^{+}TNF\alpha^{+}$ and $CD4^{+}IFN\gamma^{+}$ cells in mice infused by *E. coli* 055:HNT after DSS treatment (n = 5).

(H) Flow cytometry of $F4/80^{+}TNF\alpha^{+}$ cells in the spleen and liver of wt mice after injecting *E.coli* 055:HNT for 24 h (n = 3).

(I) CFU of *E. coli* in the spleen and liver of mice after injecting different *E. coli* strains in tail vein for 24 h. 055, *E. coli* 055:HNT; O160, *E.coli* O160:H7, G1655, *E. coli* G1655; CFT073, *E.coli* CFT073.

Scale bars = 40 μm in A. ANOVA plus post-Bonferroni analysis in A and H; Two side Student's *t*-test in E– G; Wilcoxon's test in C; analysis of variance test in D; *p<0.05, **p<0.01, and ***p<0.001; NS, no significance; R. E, relative expression. Data in A and F are represented as mean ± SEM; data in D, E, G, H, and I are represented as mean ± SD. Data in C–I are a representative of two or three independent experiments. See also Figure S6.

mice against muscle wasting and loss of fat during infections (Schieber et al., 2015). All of these may be derived from their genomic characteristics. Indeed, compared analyses of the genomes between inflamed colon tissues derived *E. coli* O160:H7 and other pathogenic and unpathogenic *E. coli* exhibit remarkable differences, especially in flagellin, rode-like proteins, and T3SS secreting system. Cytosolic PRRs (pattern recognition receptors) are critical for discriminating between pathogenic and nonpathogenic bacteria. Studies have found that cytosolic PRRs respond to patterns of pathogenesis that are often associated with virulent bacteria, such as the use of pore-forming toxins or injection of effector molecules through specialized secretion systems (von Moltke et al., 2013). The activation of NLRC4 inflammasome requires the presence of an intact type III (T3SS) or IV secretion system (T4SS) (Franchi et al., 2006). In addition, the release of T3SS PrgJ-like rod proteins into the cell cytosol can activate NLRC4. Thus, although the genetic factors of flagellin, rode-like protein, T3SS and/or IV secreting system change, these gram-negative *E. coli* may exhibit altered ability in inducing inflammatory cytokines and inflammation-associated diseases.

Our results suggest that gut epithelial cells exist in similar inflammasome complexes with macrophages to be involved in gram-negative bacteria (Qu et al., 2012). There exist multiple inflammasomes, which are broadly expressed in hematopoietic and non-hematopoietic cells, such as gut epithelial cells (Hu et al., 2010; Sellin et al., 2014), and can trigger numerous downstream responses including production of IL-1β, IL-18, and lytic cell death (Sellin et al., 2014). Despite the fact that the functional importance of inflammasomes within immune cells has been well established, the contribution of inflammasomes in non-hematopoietic cells remains comparatively understood. We here demonstrated that *E. coli* isolated from colitic tissues directly stimulate gut epithelial cells through inflammasome complexes that consisted of PKCδ, NLRC4, caspase8, and caspase11/1. Other studies also found the role of NAIP-NLRC4 (Rauch et al., 2017) and caspase4/11 (Hagar et al., 2013; Knodler et al., 2014) in gut epithelial cells. An inflammasome formed by NLRC4, ASC, and potentially caspase8 is also described in a model of enteric *S. typhimurium* infection (Rauch et al., 2017).

Although we demonstrate that inflamed *E. coli* directly and indirectly induce inflammatory macrophages through PKC δ, NLRC4, caspase8, and caspase1/11 complexes, the question is whether the inflamed *E. coli*-mediated activation of the inflammasomes in the gut and extra gut macrophages is a sufficient signal to trigger those chronic inflammatory diseases that remain unresolved. However, Kitamura et al. reported that transgenic mice expressing a constitutively active NLRC4 variant (H443P) develop an auto-inflammatory disease (Kitamura et al., 2014). Others also found that NAIP/NLRC4 inflammasome activation in MRP8+ cells is sufficient to cause systemic inflammatory diseases (Nichols et al., 2017).

Limitations of the Study

Although we analyzed the changes of cell population and subsets using flow cytometry, the exact changes of cell population and subsets, especially Ly6C+ inflammatory and anti-inflammatory macrophages in colon tissues, need to be solved through other technique(s) such as single cell analyses.

METHODS

All methods can be found in the accompanying Transparent Methods supplemental file.

DATA AND CODE AVAILABILITY

Raw 16S rRNA gene sequence data for the feces microbiota: https://www.ncbi.nlm.nih.gov/sra/PRJNA512937; Raw genome components of E. coli O160:H7: http://www.ncbi.nlm.nih.gov/bioproject/513139.

SUPPLEMENTAL INFORMATION

Supplemental Information can be found online at https://doi.org/10.1016/j.isci.2019.10.046.

ACKNOWLEDGMENTS

This research was supported by NSFC grants 91842302, 31470876, 91629102, ISF-NSFC program 31461143010, Tianjin science and technology commission (18JCZDJC35300), CAMS Innovation Fund for Medical Science (CIFMS2017-12M-2–005), a Ministry of Science and Technology grant (2016YFC1303604) and the State Key Laboratory of Medicinal Chemical Biology. We thanks Dr. Lu Gao in BGI, P. R. China for assistance in bacteria genome analyses.

AUTHOR CONTRIBUTIONS

R.Y. designed the research and wrote the paper; H. Q., Y. L., X. S., J. W. and Yingquan. L. conducted *in vivo* experiments and immunoassay, participated in study design and performed the statistical analysis; Y. G conducted *in vitro* experiments, especially immunoblotting analyses; C. Z offered patient samples and conducted some *in vivo* experiments. H. Z, L. S conducted germ-free mouse experiments; Y. X. X.Y and Yanmei, X conducted bacteria typing; Y. Z. offered assistances for the animal experiments. All authors read and approve the final manuscript.

DECLARATION OF INTERESTS

The authors declare no conflict of interest.

Received: April 1, 2019
Revised: September 13, 2019
Accepted: October 23, 2019
Published: November 22, 2019

REFERENCES

Ayres, J.S., Trinidad, N.J., and Vance, R.E. (2012). Lethal inflammasome activation by a multidrug-resistant pathobiont upon antibiotic disruption of the microbiota. Nat. Med. *18*, 799–806.

Bain, C.C., Scott, C.L., Uronen-Hansson, H., Gudjonsson, S., Jansson, O., Grip, O., Guilliams, M., Malissen, B., Agace, W.W., and Mowat, A.M. (2013). Resident and pro-inflammatory macrophages in the colon represent alternative context-dependent fates of the same Ly6Chi monocyte precursors. Mucosal Immunol. *6*, 498–510.

Becker, H.M., Apladas, A., Scharl, M., Fried, M., and Rogler, G. (2014). Probiotic Escherichia coli Nissle 1917 and commensal E. coli K12 differentially affect the inflammasome in intestinal epithelial cells. Digestion *89*, 110–118.

Blander, J.M., Longman, R.S., Iliev, I.D., Sonnenberg, G.F., and Artis, D. (2017). Regulation of inflammation by microbiota interactions with the host. Nat. Immunol. *18*, 851–860.

De Schepper, S., Verheijden, S., Aguilera-Lizarraga, J., Viola, M.F., Boesmans, W., Stakenborg, N., Voytyuk, I., Smidt, I., Boeckx, B., Dierckx de Casterle, I., et al. (2018). Self-maintaining gut macrophages are essential for intestinal homeostasis. Cell *175*, 400–415.e13.

Franchi, L., Amer, A., Body-Malapel, M., Kanneganti, T.D., Ozoren, N., Jagirdar, R., Inohara, N., Vandenabeele, P., Bertin, J., Coyle, A., et al. (2006). Cytosolic flagellin requires Ipaf for activation of caspase-1 and interleukin 1beta in salmonella-infected macrophages. Nat. Immunol. *7*, 576–582.

Franchi, L., Kamada, N., Nakamura, Y., Burberry, A., Kuffa, P., Suzuki, S., Shaw, M.H., Kim, Y.G., and Nunez, G. (2012). NLRC4-driven production of IL-1beta discriminates between pathogenic and commensal bacteria and promotes host intestinal defense. Nat. Immunol. *13*, 449–456.

Garrett, W.S., Gallini, C.A., Yatsunenko, T., Michaud, M., DuBois, A., Delaney, M.L., Punit, S., Karlsson, M., Bry, L., Glickman, J.N., et al. (2010). Enterobacteriaceae act in concert with the gut microbiota to induce spontaneous and maternally transmitted colitis. Cell Host Microbe *8*, 292–300.

Hagar, J.A., Powell, D.A., Aachoui, Y., Ernst, R.K., and Miao, E.A. (2013). Cytoplasmic LPS activates caspase-11: implications in TLR4-independent endotoxic shock. Science *341*, 1250–1253.

Hu, B., Elinav, E., Huber, S., Booth, C.J., Strowig, T., Jin, C., Eisenbarth, S.C., and Flavell, R.A. (2010). Inflammation-induced tumorigenesis in the colon is regulated by caspase-1 and NLRC4. Proc. Natl. Acad. Sci. U S A *107*, 21635–21640.

Hu, X., and Ivashkiv, L.B. (2009). Cross-regulation of signaling pathways by interferon-gamma: implications for immune responses and autoimmune diseases. Immunity *31*, 539–550.

Kayagaki, N., Warming, S., Lamkanfi, M., Vande Walle, L., Louie, S., Dong, J., Newton, K., Qu, Y., Liu, J., Heldens, S., et al. (2011). Non-canonical inflammasome activation targets caspase-11. Nature *479*, 117–121.

Kitamura, A., Sasaki, Y., Abe, T., Kano, H., and Yasutomo, K. (2014). An inherited mutation in NLRC4 causes autoinflammation in human and mice. J. Exp. Med. *211*, 2385–2396.

Knodler, L.A., Crowley, S.M., Sham, H.P., Yang, H., Wrande, M., Ma, C., Ernst, R.K., Steele-Mortimer, O., Celli, J., and Vallance, B.A. (2014). Noncanonical inflammasome activation of caspase-4/caspase-11 mediates epithelial defenses against enteric bacterial pathogens. Cell Host Microbe *16*, 249–256.

Lightfield, K.L., Persson, J., Brubaker, S.W., Witte, C.E., von Moltke, J., Dunipace, E.A., Henry, T., Sun, Y.H., Cado, D., Dietrich, W.F., et al. (2008). Critical function for Naip5 in inflammasome activation by a conserved carboxy-terminal domain of flagellin. Nat. Immunol. *9*, 1171–1178.

MacDonald, T.T., Monteleone, I., Fantini, M.C., and Monteleone, G. (2011). Regulation of homeostasis and inflammation in the intestine. Gastroenterology *140*, 1768–1775.

Man, S.M., Hopkins, L.J., Nugent, E., Cox, S., Gluck, I.M., Tourlomousis, P., Wright, J.A., Cicuta, P., Monie, T.P., and Bryant, C.E. (2014). Inflammasome activation causes dual recruitment of NLRC4 and NLRP3 to the same macromolecular complex. Proc. Natl. Acad. Sci. U S A *111*, 7403–7408.

Man, S.M., and Kanneganti, T.D. (2016). Converging roles of caspases in inflammasome activation, cell death and innate immunity. Nat. Rev. Immunol. *16*, 7–21.

Mansan-Almeida, R., Pereira, A.L., and Giugliano, L.G. (2013). Diffusely adherent Escherichia coli strains isolated from children and adults constitute two different populations. BMC Microbiol. *13*, 22.

Miao, E.A., Mao, D.P., Yudkovsky, N., Bonneau, R., Lorang, C.G., Warren, S.E., Leaf, I.A., and Aderem, A. (2010). Innate immune detection of the type III secretion apparatus through the NLRC4 inflammasome. Proc. Natl. Acad. Sci. U S A *107*, 3076–3080.

Mortha, A., Chudnovskiy, A., Hashimoto, D., Bogunovic, M., Spencer, S.P., Belkaid, Y., and Merad, M. (2014). Microbiota-dependent crosstalk between macrophages and ILC3 promotes intestinal homeostasis. Science *343*, 1249288.

Munoz, M., Eidenschenk, C., Ota, N., Wong, K., Lohmann, U., Kuhl, A.A., Wang, X., Manzanillo, P., Li, Y., Rutz, S., et al. (2015). Interleukin-22 induces interleukin-18 expression from epithelial cells during intestinal infection. Immunity *42*, 321–331.

Nichols, R.D., von Moltke, J., and Vance, R.E. (2017). NAIP/NLRC4 inflammasome activation in MRP8(+) cells is sufficient to cause systemic inflammatory disease. Nat. Commun. *8*, 2209.

Nielsen, C.M., Wolf, A.S., Goodier, M.R., and Riley, E.M. (2016). Synergy between common gamma chain family cytokines and IL-18 potentiates innate and adaptive pathways of NK cell activation. Front Immunol. *7*, 101.

Qu, Y., Misaghi, S., Izrael-Tomasevic, A., Newton, K., Gilmour, L.L., Lamkanfi, M., Louie, S., Kayagaki, N., Liu, J., Komuves, L., et al. (2012). Phosphorylation of NLRC4 is critical for inflammasome activation. Nature *490*, 539–542.

Rauch, I., Deets, K.A., Ji, D.X., von Moltke, J., Tenthorey, J.L., Lee, A.Y., Philip, N.H., Ayres, J.S., Brodsky, I.E., Gronert, K., and Vance, R.E. (2017). NAIP-NLRC4 inflammasomes coordinate intestinal epithelial cell expulsion with Eicosanoid and IL-18 release via activation of caspase-1 and -8. Immunity *46*, 649–659.

Schieber, A.M., Lee, Y.M., Chang, M.W., Leblanc, M., Collins, B., Downes, M., Evans, R.M., and Ayres, J.S. (2015). Disease tolerance mediated by microbiome E. coli involves inflammasome and IGF-1 signaling. Science *350*, 558–563.

Sekirov, I., Russell, S.L., Antunes, L.C., and Finlay, B.B. (2010). Gut microbiota in health and disease. Physiol. Rev. *90*, 859–904.

Sellin, M.E., Muller, A.A., Felmy, B., Dolowschiak, T., Diard, M., Tardivel, A., Maslowski, K.M., and Hardt, W.D. (2014). Epithelium-intrinsic NAIP/NLRC4 inflammasome drives infected enterocyte expulsion to restrict Salmonella replication in the intestinal mucosa. Cell Host Microbe *16*, 237–248.

Shouval, D.S., Biswas, A., Goettel, J.A., McCann, K., Conaway, E., Redhu, N.S., Mascanfroni, I.D., Al Adham, Z., Lavoie, S., Ibourk, M., et al. (2014). Interleukin-10 receptor signaling in innate immune cells regulates mucosal immune tolerance and anti-inflammatory macrophage function. Immunity *40*, 706–719.

Tamoutounour, S., Henri, S., Lelouard, H., de Bovis, B., de Haar, C., van der Woude, C.J., Woltman, A.M., Reyal, Y., Bonnet, D., Sichien, D., et al. (2012). CD64 distinguishes macrophages from dendritic cells in the gut and reveals the Th1-inducing role of mesenteric lymph node macrophages during colitis. Eur. J. Immunol. *42*, 3150–3166.

von Moltke, J., Ayres, J.S., Kofoed, E.M., Chavarria-Smith, J., and Vance, R.E. (2013). Recognition of bacteria by inflammasomes. Annu. Rev. Immunol. *31*, 73–106.

Winter, S.E., and Baumler, A.J. (2014). Why related bacterial species bloom simultaneously in the gut: principles underlying the 'Like will to like' concept. Cell Microbiol *16*, 179–184.

Wynn, T.A., Chawla, A., and Pollard, J.W. (2013). Macrophage biology in development, homeostasis and disease. Nature *496*, 445–455.

Zigmond, E., Varol, C., Farache, J., Elmaliah, E., Satpathy, A.T., Friedlander, G., Mack, M., Shpigel, N., Boneca, I.G., Murphy, K.M., et al. (2012). Ly6C hi monocytes in the inflamed colon give rise to proinflammatory effector cells and migratory antigen-presenting cells. Immunity *37*, 1076–1090.

ISCI, Volume *21*

Supplemental Information

Induction of Inflammatory Macrophages in the Gut and Extra-Gut Tissues by Colitis-Mediated *Escherichia coli*

Houbao Qi, Yunhuan Gao, Yuanyuan Li, Jianmei Wei, Xiaomin Su, Chunze Zhang, Yingquan Liu, Hua Zhu, Lei Sui, Yanwen Xiong, Xi Yang, Yanmei Xu, Yuan Zhang, and Rongcun Yang

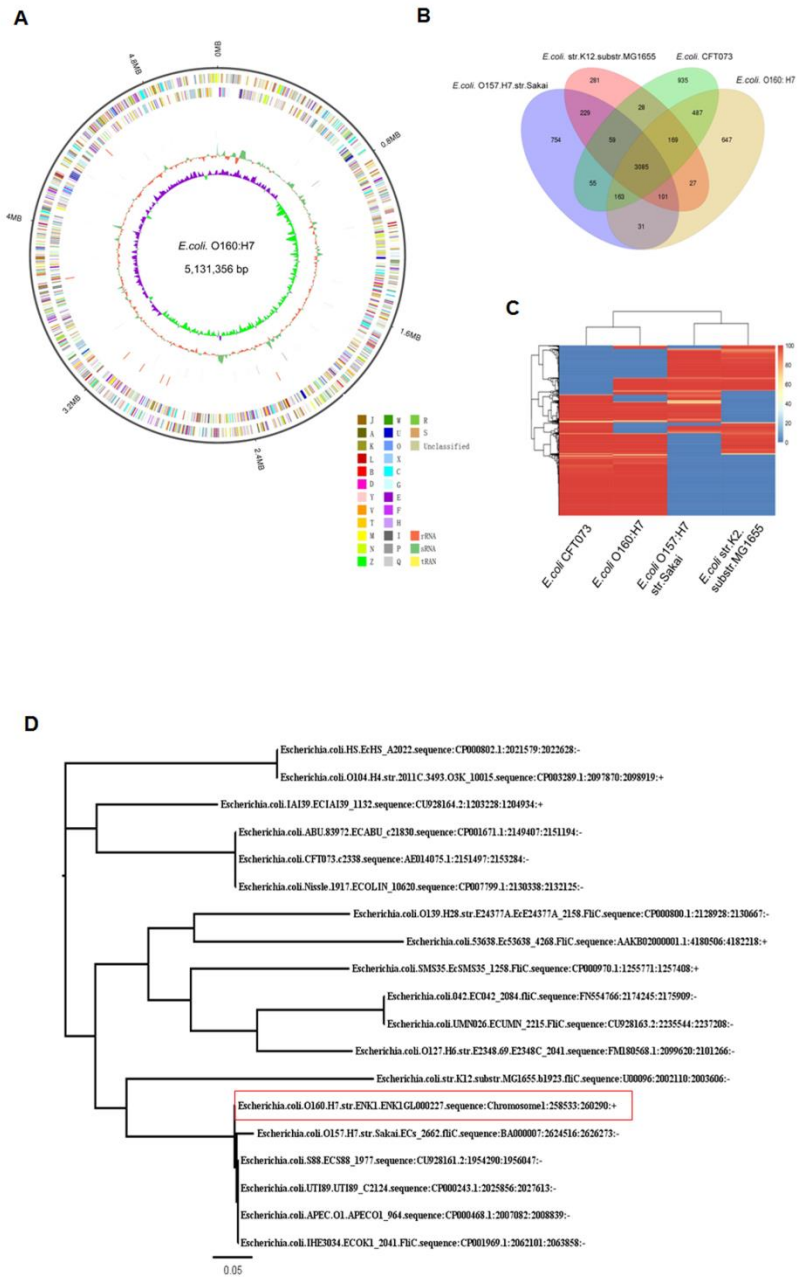

Figure S1. Characteristics of *E. coli* O160: H7 genome, Related to Figure 1.

(A) Circular representation of *E. coli* O160: H7 genome. From outer to inner :1, Genome Size; 2, Forward Strand Gene, colored according to cluster of orthologous groups (COG) classification; 3, Reverse Strand Gene, colored according to cluster of

orthologous groups (COG) classification; 4, Forward Strand ncRNA; 5, Reverse Strand ncRNA; 6, Repeat; 7, GC; 8, GC-SKEW. J, Translation, ribosomal structure and biogenesis; A, RNA processing and modification; K, Transcription；
L, Replication, recombination and repair; B, Chromatin structure and dynamics ; D, Cell cycle control, cell division, chromosome partitioning； Y, Nuclear structure;
V, Defense mechanisms; T, Signal transduction mechanisms； M, Cell wall/membrane/envelope biogenesis; N, Cell motility; Z, Cytoskeleton;
W, Extracellular structures; U, Intracellular trafficking, secretion, and vesicular transport; O, Posttranslational modification, protein turnover, chaperones ； X,

Mobilome: prophages, transposons; C, Energy production and conversion; G, Carbohydrate transport and metabolism; E, Amino acid transport and metabolism;
F, Nucleotide transport and metabolism; H,Coenzyme transport and metabolism;
I, Lipid transport and metabolism; P, Inorganic ion transport and metabolism; Q, Secondary metabolites biosynthesis, transport and catabolism; R, General function prediction only; S, Function unknown.

(B) The pan-gene Venn graph of *E. coli* O160:H7 (ENK1), *E.coli* O157.H7.str.Sakai , *E.coli*.str.K12.substr.MG1655 and *E.coli* CFT073. Each ellipse represent one strain, the number in the ellipse means the only cluster number. One cluster have the genes that more than 50 percent identity and less than 0.3 length diversity.

(C) Dispensable gene heat map in each strain. Left, dispensable gene cluster; Top, strain cluster; The similarities of gene, the middle with different color represent different coverage by heat map; Color/depth, top left pic. Below, each strain name. *E. coli* O160:H7 (ENK1).

(D) FliC phylogenetic analysis. The web based program Phylogeny.fr was used for phylogenetic analysis of the *fliC* gene sequence from *E. coli* O160:H7 as compared to publicly available *fliC* gene sequences from pathogenic and non-pathogenic *E. coli* strains. *E. coli* O160:H7 is marked.

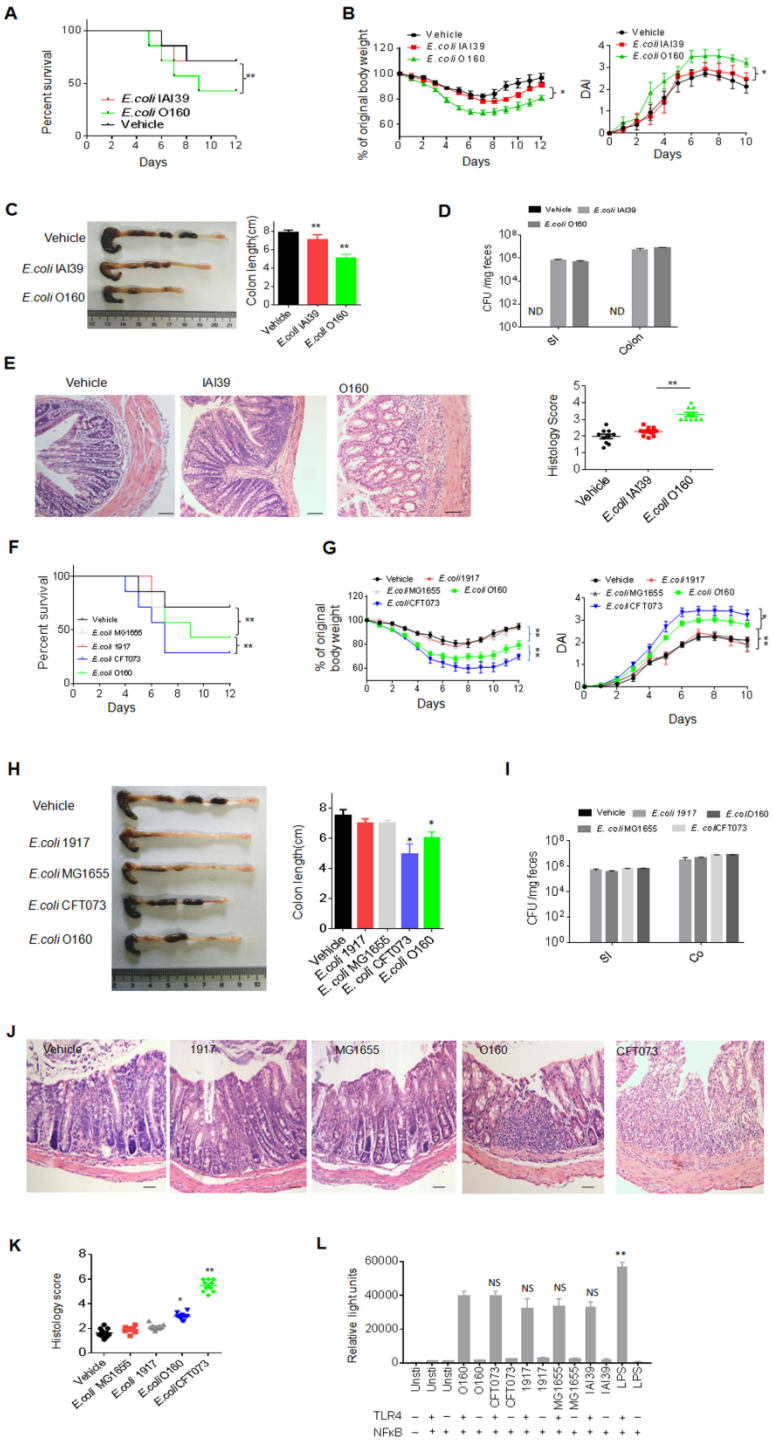

Figure S2. *E. coli* O160:H7 is different from other *E. coli* strains in promoting sensitivity to DSS-mediated colitis, Related to Figure 1.

(A and B) Survival rate (A), body weight and disease activity index (B) were monitored in mice infused by *E. coli* O160:H7 strain and *E. coli* IAI39 (isolated from mice) under DSS (n=12).

(C) Length of colon were monitored at day 7 after the start of DSS in mice infused by *E. coli* O160:H7 strain and *E. coli* IAI39 (n=6).

(D) CFU of *E. coli* in small intestine and colon of mice infused by *E. coli* O160:H7 and *E. coli* IAI39 (n=6).

(E) H&E staining and histological scores of colon tissues in mice infused by *E. coli* O160:H7 strain or *E. coli* IAI39 after DSS-treatment (n=6).

(F and **G**) Survival rate (F), body weight and disease index (G) were monitored in mice infused by *E. coli* O160:H7, *E. coli* G1655, *E. coli* CFT0735 or *E. coli* 1917 under DSS (n=12).

(H) Length of colon were monitored at day 7 after the start of DSS (n=6).

(I) CFU of *E. coli* in small intestine and colon of mice infused by *E. coli* O160:H7, *E. coli* G1655 and *E.coli.* CFT0735 or *E. coli* 1917..

(J and **K**) H&E staining (J) and histological scores (K) of colon tissues in mice infused by *E. coli* O160:H7 strain, *E. coli* G1655, *E.coli* CFT0735 or *E. coli* 1917 after DSS-treatment.

(L) NF-κB activity in TLR4 expressed 293T cells after exposed to different *E. coli* O160:H7, *E. coli* G1655 and *E. coli* CFT0735 or *E. coli* 1917. NF-κB activity was detected using NF-κB reporter analysis system.

Scale bars=40 μm; Wilcoxon's test in A and F; Analysis of variance test in B and G; ANOVA plus post-Bonferroni analysis in C, E, K and L; *P<0.05, **P<0.01 and ***P<0.001; NS, no significance; R. E, relative expression. Data in B, C, D, G, H, I and L are represented as mean+/-SD; Data in E and K are represented as mean+/-SEM. Data are a representative of two or three independent experiments.

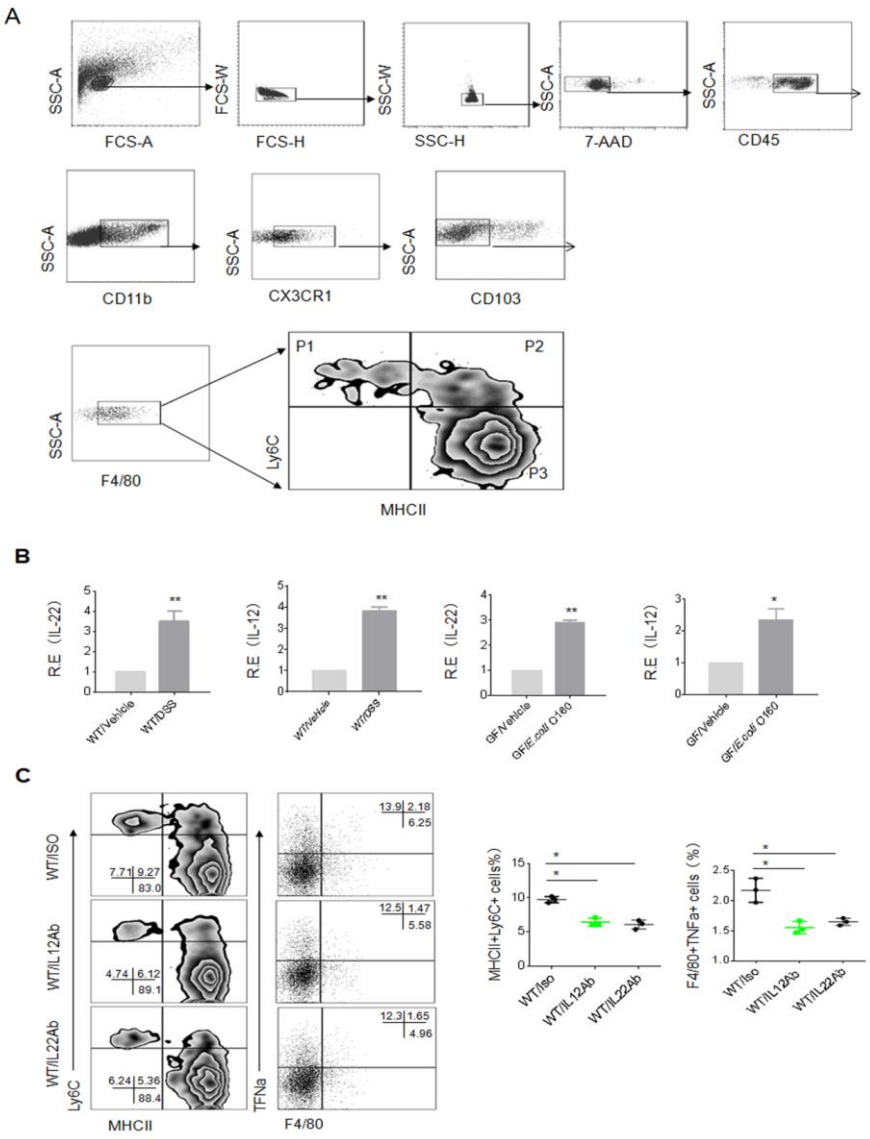

Figure S3. IL-12 and IL-22 affect the accumulation of inflammatory macrophages, Related to Figure 2 and 3.

(A) Gating strategy was based on Bain *et al.* who showed that distinct macrophages subsets can be isolated without using CX3CR1-GFP reporter mice (Bain et al., 2013) and Shouval, *Immunity*. 2014). We performed some modifications to this method: following initial gating on live CD45+ cells after eliminating double and dead cells using FCS-W, SSC-W and 7-AAD staining, we gated on F4/80^{+} CD103^{-} cells after gating CD11B and CXCR1, and finally gated on Ly6C and MHCII.

(B) QRT-PCR of IL-12 and IL-22 in the colon tissues of and DSS-treated mice or *E. coli* infused mice (n=3).

(C) Flow cytometry of inflammatory macrophages in the colon LP of DSS-treated mice injected neutralizing IL-12 or IL-22 Ab (n=3).

Two side Student's *t*-test in B; ANOVA plus post-Bonferroni analysis in C. *P<0.05, **P<0.01 and ***P<0.001; NS, no significance; R. E, relative expression. Data in B and C are represented as mean+/-SD. Data are a representative of three independent experiments.

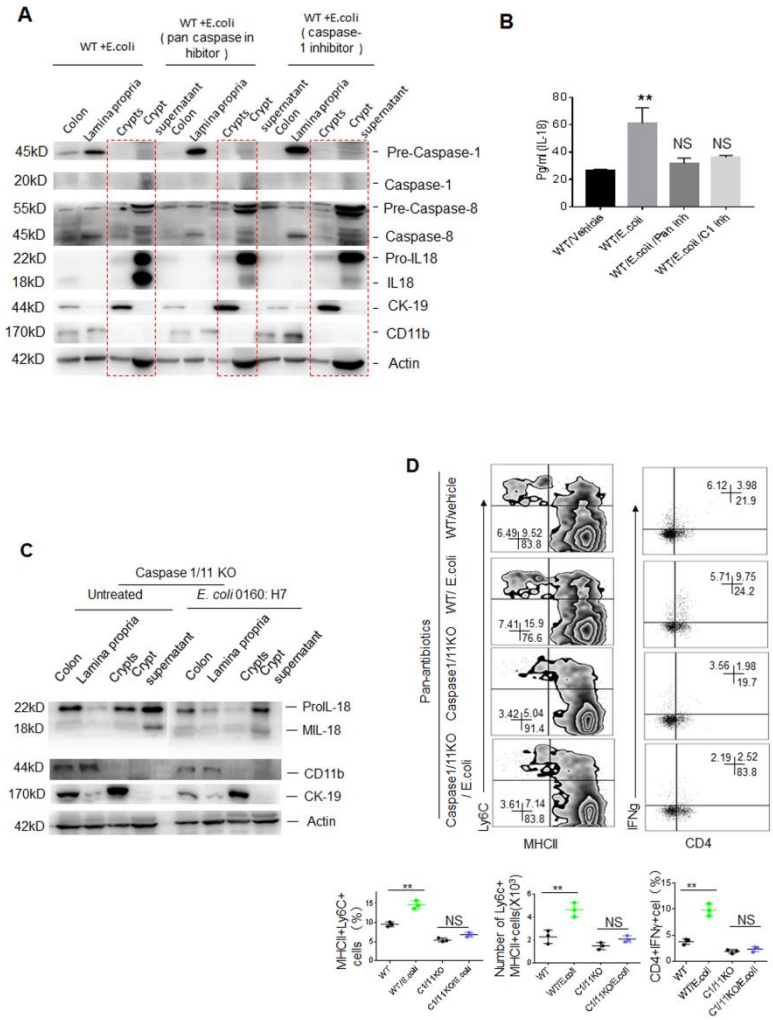

Figure S4. *E. coli* O160: H7 mediated inflammatory macrophages needs caspase-1 in gut epithelial cells, Related to Figure 5.

(A) Immunoblotting of pre-caspase-1, mature caspase-1, pre-casepase-8, mature caspase-8, pro-IL-18 and mature IL-18 in colon tissues, lamina propria, crypts and crypt supernatants of wt mice after exposed to E. coli with or without pan-caspases and caspase 1 inhibitors for one hour.

(B) ELISA of IL-18 in the supernatants of colon epithelial cells after exposed to different *E. coli* with or without pan-caspase and caspase 1 inhibitor for one hour.

(C) Immunoblotting of pro-IL-18 and mature IL-18 in colon tissues, lamina propria, crypts and crypt supernatants of caspase 1/11 KO mice after exposed to E. coli for one hour.

(D) Flow cytometry of inflammatory macrophages and $CD4^{+}IFN\gamma^{+}$in the LP of colon tissues of caspase 1/11 (C1/11) KO mice infused *E. coli* O160 (n=3)

ANOVA plus post-Bonferroni analysis in B and D; *P<0.05, **P<0.01 and ***P<0.001; NS, no significance; R. E, relative expression. Data in B and D are represented as mean+/-SD. Data are a representative of three independent experiments.

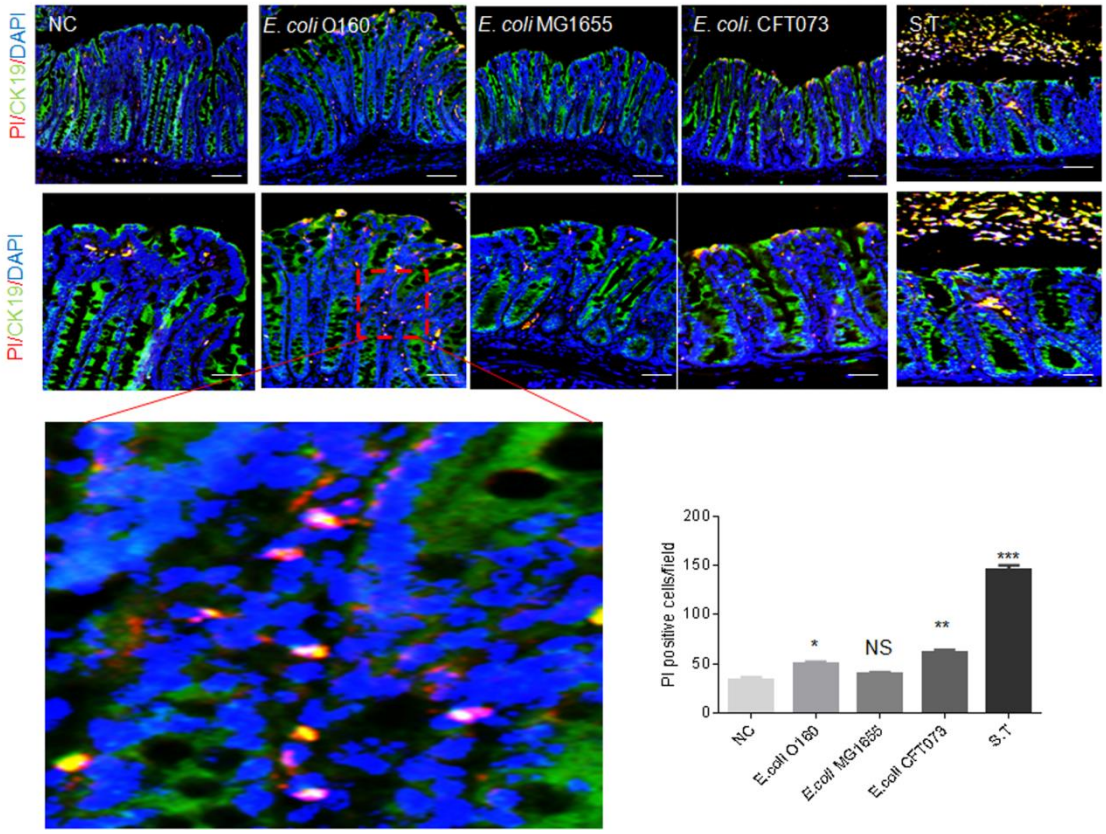

Figure S5. *E. coli* O160: H7 may cause pyroptosis of gut epithelial cells, Related to Figure 5.

Staining of propidium and fluorescent CK19, marker of gut epithelial cells in mice infused using *E. coli* O160:H7, *E.coli* G1655, *E. coli* CFT073 and positive control Salmonella Typhimurium (ST, 1×10^9/mouse). For propidium iodide staining, mice were injected with 100μg/mouse propidium iodide intravenously 10 minutes before sacrifice (Rauch et al, Immunity, 2017). Data are represented as mean+/-SEM. Scale bars=20 μm (upper) or 40 μm (lower). ANOVA plus post-Bonferroni analysis; *P<0.05, **P<0.01 and ***P<0.001; NS, no significance;

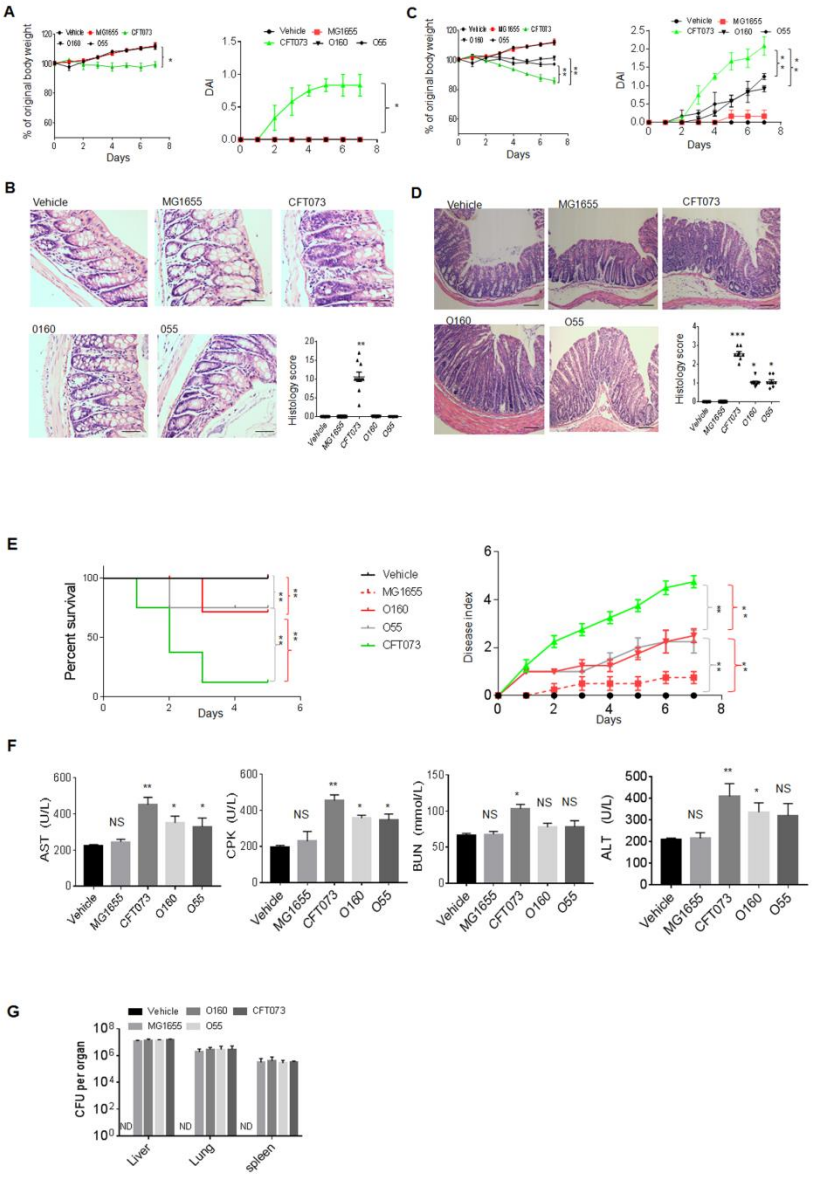

Figure S6. *E. coli* O160:H7 only cause weaker responses as compared to pathogenic *E. coli*, Related to Figure 7.

(A) Body weight and disease activity index in *wt* mice after orally infusing different kinds of *E. coli* .

(B) H&E staining of colon tissues in *wt* mice after infusing different *E. coli*.

(C) Body weight and disease activity index of different kinds of *E. coli* orally infused mice, which were treated using pan-anti-biotics.

(D) H&E staining of colon tissues in pan-anti-biotics treaed mice after infusing *E. coli*

(E) Survival rate and disease activity index of mice after in vein injecting different kinds of bacteria (1×10^8/mice) (n=12)

(F) The concentration of ASK, CPK, BUN and ALT in peripheral blood of mice after in vein injecting different kinds of bacteria for 3days (n=8).

(G) CFU in different tissues and organs of mice after injecting different kinds of bacteria (1×10^8/mice) (n=8) for 3 days.

1655, *E. coli* G1655; CFT073, *E.coli* CFT073; O160, *E. coli* O160:H7; 055, *E. coli* 055: HNT. Scale bars=40 μm. Analysis of variance test in A, C and E (right); Wilcoxon's test in E (left); ANOVA plus post-Bonferroni analysis in B, D and F; *P<0.05, **P<0.01 and ***P<0.001; NS, no significance; R. E, relative expression. Data in A, C, E (right), F and G are represented as mean+/-SD; Data in B and D are represented as mean+/-SEM. in Data are a representative of three independent experiments.

Table S1 Characteristics of isolated E. coli from colon tissues, Related to Figure 1.

Transparent Methods

Mice

Four-to six-week-old male or female C57BL/6 mice were obtained from Nanjing Animal Center. IL-18-/- mice was from Prof. Meng, University of Chinese Academy of Sciences, shanghai; Caspase1/caspase -11-/- and NLRC4-/- were from Prof. Shao, National Institute of Biological Sciences, Beijing; IFNγ-/- mice was offered by Prof. Lian, University of Science and Technology of China, Hefei. All experimental litters were bred and maintained under specific pathogen-free (SPF) conditions in the Animal Center of Nankai University. All experimental variables such as husbandry, parental genotypes and environmental influences were carefully controlled. Male, 6-8 weeks old mice were used in this study except for special indication.

C57BL/6 germ-free (GF) mice were generated by Institute of Laboratory Animal Science, Peking Union Medical College (PUMC). All experiments in GF mice were performed in the Institute of Laboratory Animal Science, Peking Union Medical College (PUMC).

All procedures were conducted according to the Institutional Animal Care and Use Committee of the Model Animal Research Center. Animal experiments were approved by the Institute's Animal Ethics Committee of Nankai University.

Patients

Eighty inflammatory bowel disease (IBD) patients (10 active Crohn's disease (CD), 20 inactive CD, 50 active ulcerative colitis (UC)) and 50 patients with colitic cancer

who regularly visited the Tianjin people hospital (Tianjin, China) from 2017 to 2018 were recruited to the study. The diagnosis of IBD was based on standard clinical, endoscopic, radiological and histological criteria(Ouyang et al., 2006). The control group consisted of sex- and age-matched healthy subjects. Patients with IBD who met any of the following criteria were excluded: (1) use of antibiotics, probiotics or prebiotics in the 3-month period immediately preceding the sampling time point; (2) current infectious diarrhea; and (3) malignancy. UC activity was evaluated using the Mayo score (D'Haens et al., 2007); Active UC was defined as UC disease activity index >2. Activity of CD was scored by Crohn's disease activity index (CDAI) (Geubel et al., 1976); Active CD was defined as a CDAI > 150. Written informed consent was obtained from all subjects prior to their enrollment.

The study was approved by the Ethics Committee at the Tianjin People Hospital, Tianjin, China. It was conducted in accordance with guidelines expressed in the Declaration of Helsinki.

Bacterial strains

E. coli O160: H7 and *E. coli* IAI139 were respectively isolated from DSS-mediated colitic tissue and colon contents of mice. *E.coli* O55: HNT was also isolated from colitic tissues of patients with inflammatory bowel disease.

*E.coli*str.K12.substr.MG1655, *E.coli* Nissle. 1917 and DH5α was from ATCC; *E. coli* CFT073 were from Chinese Center for Disease Control and Prevention. *Samonella* typhimurium (ATCC14028) was from Pro. Guo, College of Life Science, Wuhan University. These bacteria were grown in LB media

shaking at 37^{o}C overnight and stored in 25% glycerol frozen stocks and used for experiments.

Mouse models

For dextran sodium sulfate (DSS) induced colitis, DSS induced colitis was performed according to our previously reported method (Cao et al., 2016) with modification. Briefly, mice received 2.5% (*wt* mice), 2.2% (Pan-antibiotics treated mice) (wt/vol) DSS (40,000 kDa; MP Biomedicals) or at the indicated dose in their drinking water for 7 days, then switched to regular drinking water. The amount of DSS water drank per animal was recorded and no differences in intake between strains were observed. For survival studies, mice were followed for 12 days post start of DSS-treatment. Mice were weighed every other day for the determination of percent weight change. This was calculated as: % weight change = (weight at day X-day 0 / weight at day 0) × 100. Animals were also monitored clinically for rectal bleeding, diarrhea, and general signs of morbidity, including hunched posture and failure to groom. For microbiota transplantation, germ-free (GF) mice were orally administered 200 μl of fecal suspension or 1×10^{9} bacteria (once/week). In *wt* mice, mice were first treated with pan-antibiotics (ampicillin (A, 1 g/L, Sigma), vancomycine (V, 0.5g/L, Sigma), neomycin sulfate (N, 1 g/L, Sigma), and metronidazole (M, 1g/L, Sigma)) via the drinking water for one week (sometime longer than one week) and then orally administered 200 μl of fecal suspension or 1×10^{9} bacteria (once/week). To confirm the elimination of bacteria, stools were collected from antibiotic-treated and untreated mice and cultured in anaerobic and aerobic condition. For oral infection, *E. coli* overnight grew in LB media shaking at 37 ℃. Mice were gavaged with 1×10^{9} *E. coli*

in 200 μl of sterile PBS. Mice were sacrificed at the indicated days. Representative colon tissues were embedded in paraffin for hematoxylin/eosin (H&E) staining or embedded in OCT compound (Tissue-Tek, Sakura, Torrance, CA) and frozen over liquid nitrogen for immuno-staining.

Disease activity index (DAI) and histological scores were assessed according to following methods. Disease activity index was the average of these scores: (combined score of stool consistency, bleeding and weight loss)/3 (Tang et al., 2015). Diarrhea was scored daily as follows: 0, normal; 2, loose stools; 4, watery diarrhea. Blood in stool was scored as follows: 0, normal; 2, slight bleeding; 4, gross bleeding. Weight loss was scored as follows: 0, none; 1, 1%-5%; 2, 5%- 10%; 3, 10%-15%; 4, >15%. Disease activity index was the average of these scores: (combined score of stool consistency, bleeding and weight loss)/3. For histological evaluation, histology was scored as follows: epithelium (E), 0=normal morphology; 1=loss of goblet cells; 2=loss of goblet cells in large areas; 3=loss of crypts; 4=loss of crypts in large areas; and infiltration (I), 0=no infiltrate; 1=infiltrate around the crypt basis; 2=infiltrate reaching the lamina (L) muscularis mucosae; 3=extensive infiltration reaching the L muscularis mucosae and thickening of the mucosa with abundant oedema; 4=infiltration of the L submucosa. Total histological score was given as E+I (Tang et al., 2015).

For *in vivo* injection, *E. coli* overnight grew in LB media shaking at 37 ℃. Mice were injected intravenously with 5×10^8 live or dead bacteria in PBS, and then survival (time to moribund) were detected. Disease indexes (DI) were scored using a quantitative scale that integrated four cardinal signs of systemic toxicity (piloerection,

ocular discharge, lethargy, and diarrhea; each scored from zero to three) (Liu et al., 2011).

For blocking experiments, mice or *E. coli* transplanted mice were injected i.p. with the anti-IFN-γ mAb (100 μg/g body weight), anti-IL18 mAb (100 ug/g), anti-IL22 mAb (100ug/g), anti-IL12 mAB(100 ng/g) or control isotypic antibody (100 ng/g) at day 1 and day 3, and then lamina propria cells were analyzed at day 6.

Analyses of gut microbiota

For gut microbiota analyses, the DSS-treated mice and unmolested control littermate wt mice were reared in different cages. Gut microbiota was analyzed by Majorbio Biotechnology Company (Shanghai, China) using primers that target to V3-V4 regions of 16S rRNA. Once PCR for each sample, the amplicons were purified using the QIAquick PCR purification kit (Qiagen Valencia, CA), quantified, normalized, and then pooled in preparation for emulsion PCR followed by sequencing using Titanium chemistry (Roche, Basel Switzerland) according to the manufacturer's protocol. Operational Taxonomic Unit (OTU) analysis was performed as follows: sequences were processed (trimmed) using the Mothur software and subsequently clustered at 97% sequence identity using cd-hit to generate OTUs. The OTU memberships of the sequences were used to construct a sample-OTU count matrix. The samples were clustered at phylum, genus and OTU levels using the sample-phylum, sample-genus and sample-OTU count matrices respectively. For each clustering, Morisita-Horn dissimilarity was used to compute a sample distance matrix from the initial count matrix, and the distance matrix was subsequently used to generate a hierarchical clustering using Ward's minimum variance method. The

Wilcoxon Rank Sum test was used to identify OTUs that had differential abundance in the different sample groups.

For colony analysis of the gut tract and extra-gut tissues, the homogenized colon and extra-colon tissues from DSS treated, unmolested mice or *E. coli* infected wt or GF mice were harvested, and then serially diluted the homogenates and plated them on bacterial medias that support the growth of *E. coli* such as LB. We then incubated the plates aerobically at 37 ℃ for 24 h, after which we counted colonies, classified based on colony appearance and subjected them to 16S rDNA colony PCR and sequencing. For colony PCR, we resuspended colonies in sterile PBS, boiled for 10 min at 100 ℃ and then V1-V9 regions were analyzed by PCR with the universal bacterial primers 27F (5′-AGAGTTTGATCCTGGCTCAG-3′) and 1492R (5′-GGTTACCTTGTTACGACTT-3′) (DeSantis et al., 2007). PCR was performed on a Bio-Rad iCycler using an annealing temperature of 51 ℃ and the following conditions: 95 ℃ (5 min), followed by 30 cycles of 95 ℃ (30 s), annealing (1 min), 72 ℃ (2 min), and a final extension at 72 ℃ (10 min). Reactions were then subjected to a PCR cleanup using the QIAquick PCR Purification Kit (Qiagen) and sequenced using the 27F and 1492R primers (Beijing Genomics Institute (BGI)). We classified the sequences using Microbial Nucleotide BLAST (https://blast.ncbi.nlm.nih.gov/Blast.cgi).

For serotyping , previously reported methods were used in this study (Bai et al., 2016). Briefly, **t**he O antigen was initially screened using the O-genotyping PCR method to identify and classify the *E.coli* O sero groups. The complete *E.coli* O antisera (O1-O188; Statens Serum Institut, Hillerød,Denmark) were used to confirm the PCR results. The isolates were referred as O-untypable if they did not react with

any O antisera. The entire coding sequence of *fliC* was amplified by PCR using the primers:F-FLIC1(5′- ATGGCACAAGTCATTAATACCCAAC-3′) and R-FLIC2(5′-CTAACCCTGCAGCAGAGACA-3′). Then, the PCR products were sequenced and compared to a publicly available CGE Serotype Finder database (http://cge.cbs.dtu.dk/ services/) to determine the H type of each isolate. The isolate was H-untypable if *fliC* was negative by PCR.

For multilocus sequence typing (MLST), previously reported methods were used (Bai et al., 2016). Briefly, defined fragments of the seven mouse keeping genes (i.e., *adk*, *icd*, *fumC*, *recA*, *mdh*, *gyrB*, and *purA*) were amplified and sequenced according to the *E.coli* MLST website (http://mlst.warwick.ac.uk/mlst/dbs/Ecoli). Sequences types (STs) for each isolate were assigned based on the allelic profile of the seven house keeping genes. A neighbor-joining tree was constructed by MEGA 6 based on the concatenated sequences of the seven house keeping genes, and used to analyze the phylogenetic relationships among strains.

Analyses of *E. coli* O160: H7

For genome sequencing and assembly of *E. coli* O160: H7, the mouse strain ENK1 (*E. coli* O160: H7) genome was sequenced using a PacBio RS II platform and Illumina HiSeq 4000 platform in the Beijing Genomics Institute (BGI, Shenzhen, China). Four SMRT cells Zero-Mode Waveguide arrays of sequencing were used by the PacBio platform to generate the subreads set. PacBio subreads (length < 1 kb) were removed. The program Pbdagcon (https://github.com/PacificBiosciences/pbdagcon) was used for self correction. Draft genomic unitigs, which are uncontested groups of fragments, were assembled using the Celera Assembler against a high quality corrected circular

consensus sequence subreads set. To improve the accuracy of the genome sequences, GATK (https://www.broadinstitute.org/gatk/) and SOAP tool packages (SOAP2, SOAPsnp, SOAPindel) were used to make single-base correction. To trace the presence of any plasmid, the filtered Illumina reads were mapped using SOAP to the bacterial plasmid database (http://www.ebi.ac.uk/genomes/plasmid.html).

For genome component prediction, gene prediction was performed on the *E.coli*O160:H7 (ENK1) genome assembly by glimmer3 (http://www.cbcb.umd.edu/software/glimmer/) with Hidden Markov models. tRNA, rRNA and sRNAs recognition made use of tRNAscan-SE, RNAmmer, and the Rfam database. The tandem repeats annotation was obtained using the Tandem Repeat Finder (http://tandem.bu.edu/trf/trf.html), and the minisatellite DNA and microsatellite DNA were selected based on the number and length of repeat units .The Genomic Island Suite of Tools (GIST) was used for genomicis lands analysis (http://www5.esu.edu/cpsc/bioinfo/software/GIST/) with IslandPath-DIOMB, SIGI-HMM, IslandPicker method. Prophage regions were predicted using the PHAge Search Tool (PHAST) web server (http://phast.wishartlab.com/) and CRISPR identification using CRISPRFinder.

For gene annotation and protein classification, the best hit abstracted using Blast alignment tool for function annotation. Seven databases which are KEGG (Kyoto Encyclopedia of Genes and Genomes), COG (Clusters of Orthologous Groups), NR(Non-Redundant Protein Database databases), Swiss-Prot,and GO (Gene Ontology), TrEMBL, EggNOG are used for general function annotation. Four databases for pathogenicity and drug resistance analysis. Virulence factors and resistance gene were identified based on the core dataset in VFDB (Virulence Factors of Pathogenic Bacteria) and ARDB (Antibiotic Resistance

Genes Database) database, other two are PHI (Pathogen Host Interactions) and (Carbohydrate-Active enZYmes Database). Type III secretion system effector proteins were detected by EffectiveT3.

For comparative genomics and phylogenetic analysis, the synteny of *E. coli* O160: H7 and other pathogenic and non-pathogenic *E. coli* strains was performed using MUMmer and BLAST Core/Pan genes of *E. coli* O160: H7 and other pathogenic and non-pathogenic *E. coli* strains were clustered by the CD-HIT rapid clustering of similar proteins software with a threshold of 50% pairwise identity and 0.7 length difference cutoff in amino acid. Gene family was constructed by the gene of *E. coli* O160: H7, other pathogenic and non-pathogenic *E. coli* strains, integrating multi software: align the protein sequence in BLAST and eliminate the redundancy by solar and carry out gene family clustering treatment for the alignment results with Hcluster_sg software. The phylogenetic tree is constructed by the TreeBeST using the method of NJ.

Reference sequences were respectively from:

E. coli strain Nissle *1917* https://www.ncbi.nlm.nih.gov/bioproject/447975 ;

E. coli O157:H7 strain https://www.ncbi.nlm.nih.gov/bioproject/479590 ;

E. coli CFT073 https://www.ncbi.nlm.nih.gov/bioproject/313;

Escherichia coli str. K-12 substr.

MG1655 https://www.ncbi.nlm.nih.gov/bioproject/485867;

E. coli E24377A ETEC NC_009801

https://www.ncbi.nlm.nih.gov/bioproject/13960;

E. coli 53638 EIEC AAKB00000000 _

https://www.ncbi.nlm.nih.gov/bioproject/15639;

E. coli APEC O1 CP000468 https://www.ncbi.nlm.nih.gov/bioproject/16718; E.

coli IAI39 ExPEC https://www.ncbi.nlm.nih.gov/bioproject/33411;

E.coli 042 EAEC FN554766 https://www.ncbi.nlm.nih.gov/bioproject/40647;

Escherichia coli O113:H21 str. CL-3

https://www.ncbi.nlm.nih.gov/bioproject/72243;

Escherichia coli strain VTH-15 https://www.ncbi.nlm.nih.gov/nuccore/GQ423574.1

Escherichia coli 042 https://www.ncbi.nlm.nih.gov/bioproject/40647

Escherichia coli ABU 83972 https://www.ncbi.nlm.nih.gov/bioproject/38725

Escherichia coli O127:H6 str. E2348/69

https://www.ncbi.nlm.nih.gov/bioproject/285331

Escherichia_coli_HS https://www.ncbi.nlm.nih.gov/bioproject/13959

Escherichia_coli_S88 https://www.ncbi.nlm.nih.gov/bioproject/33375

Escherichia_coli_IHE3034 https://www.ncbi.nlm.nih.gov/bioproject/43693

Escherichia_coli_UTI89 https://www.ncbi.nlm.nih.gov/bioproject/16259

Escherichia coli IAI39 https://www.ncbi.nlm.nih.gov/bioproject/59381

Escherichia_coli_SMS-3-5 https://www.ncbi.nlm.nih.gov/bioproject/19469

Escherichia coli STEC_B2F1 https://www.ncbi.nlm.nih.gov/bioproject/48273

Escherichia_coli_UMN026 https://www.ncbi.nlm.nih.gov/bioproject/62981

Escherichia_coli_O111_H-_str._11128 _

https://www.ncbi.nlm.nih.gov/bioproject/32513

Escherichia coli O113:H21 str. CL-3

https://www.ncbi.nlm.nih.gov/bioproject/72243

Escherichia coli strain VTH-15 https://www.ncbi.nlm.nih.gov/nuccore/GQ423574.1

Out group: Legionella pneumophila

https://www.ncbi.nlm.nih.gov/nuccore/NC_006368.1

Cell isolation and flow cytometry

For the staining of lamina propria (LP) lymphocytes, colon or small intestine were isolated, cleaned by shaking in ice-cold PBS four times before tissue was cut into 1 cm pieces. The epithelial cells were removed by incubating the tissue in HBSS with 2 mM EDTA for 30 min with shaking. The LP cells were isolated by incubating the tissues in digestion buffer (DMEM, 5% fetal bovine serum, 1 mg/ ml Collagenase IV (Sigma-Aldrich) and DNase I (Sigma-Aldrich) for 40 min at 37^{o}C with shaking. The digested tissues were then filtered through a 40-mm filter. Cells were resuspended in 10 ml of the 40% fraction of a 40: 80 Percoll gradient and overlaid on 5 ml of 80% fraction in a 15 ml Falcon tube. Percoll gradient separation was performed by centrifugation for 20 min at 1,800 rpm at room temperature. LP cells were collected at the interphase of the Percoll gradient, washed and resuspended in medium, and then stained and analyzed by flow cytometry. Single-cell suspensions of MLNs, PPs and spleen were prepared by mashing in a cell strainer (70 mm).

For analysis of different immune cell populations, the cells were washed with staining buffer containing PBS, 2% FBS, 1 mM EDTA and 0.09% NaN3 and surface staining was performed with FITC, PE, APC, PercP/cy5.5, BV421, BV605, APC/Cy7 or Alexa fluor 700 -labeled anti-CD4, CD11c, MHCII, F4/80, CD11b, Ly6C, CD45, CX3CR1, CD103, TNFα, IFNγ, IL-17A, Foxp3, CD103 and Ki67 antibodies and analyzed using FACScan flow cytometry (Su et al., 2014). Gating strategy was based on Bain *et al.* who showed that distinct macrophages subsets can be isolated without using CX3CR1-GFP reporter mice (Bain et al., 2013; Shouval et al., 2014). We performed some modifications to this method: following initial gating on live CD45^{+} cells we gated on CX3CR1^{+}CD11b^{+} CD103^{-}F4/80^{+} cells, and then analyse Ly6C and MHCII (Bain et al., 2013); Double cells or other unseparated cells were gated out

based on SSC and FSC. Dead cells were eliminated through 7-AAD staining.

For intracellular staining, the cells were cultured and stimulated for 6 hrs with 50ng/ml phorbol 12-myristate 13-acetate (PMA, Sigma) and 1 μg/ml ionomycin (Sigma) in the presence of GolgiStop (10 ng/ml, BD Biosciences). After incubation for 6 hrs, cells were washed in PBS, and then fixed in Cytofix/Cytoperm, permeabilized with Perm/Wash buffer (BD Biosciences), and stained with FITC-, PE-, APC or PerCP/Cy5.5 -conjugated antibodies. Meanwhile, dead cells were eliminated through 7-AAD staining.

Staining

For hematoxylin/eosin (H&E) staining, previously reported methods were used in this experiment (Cao et al., 2016; Su et al., 2014)**.** Briefly, the entire colon was excised to measure the length of the colon and then were fixed in 4% (w/v) paraformaldehyde buffered saline and embedded in paraffin, 5 μm sections colon sections were cut and stained with H&E.

For immunostaining, immunostaining was performed according to our previous method(Cao et al., 2016; Su et al., 2014). 5-μm-thick sections were prepared from the frozen tissue and fixed in acetone (−20°C) for 10 min. After rehydration in PBS for 5 min and further washing in PBS, tissue sections were blocked with 1% (w/v) BSA and 0.2% (w/v) milk powder in PBS (PBS-BB). The primary antibody was added in PBS-BB and incubated overnight at 4 ℃. After PBS washing (three times, 5 min each), tissue was detected with DAB kit or fluorescence labeled second antibody. Nuclei were stained by DAPI.

For fluorescent *in situ* hybridization (FISH), mucus immune-staining was paired with fluorescent *in situ* hybridization (FISH) in order to analyze bacteria localization

at the surface of the intestinal mucosa according to reported method (Chassaing et al., 2016; Vaishnava et al., 2011). In brief, the ileum and colonic tissues (proximal colon, second centimeters from the caecum) containing fecal material were placed in methanol-Carnoy's fixative solution (60% methanol, 30% chloroform, 10% glacial acetic acid) for a minimum of 3 hrs at room temperature. Tissue were then washed in methanol, ethanol, ethanol/xylene (1:1) and xylene, followed by embedding in paraffin with a vertical orientation. 5-µm sections were cut and dewaxed by preheating at 60 ^{o}C for 10 min, followed by bathing in xylene at 60 ^{o}C for 10 min, xylene at room temperature for 10 min and 99.5% ethanol for 10 min. The hybridization step was performed at 50 ^{o}C overnight with an probe diluted to a final concentration of 0.01µg/mL in hybridization buffer (20mM Tris-HCl, pH7.4, 0.9M NaCl, 0.1% SDS, 20% formamide). After washing for 10 min in wash buffer (20mMTris-HCl, pH7.4, 0.9MNaCl) and 10 min in PBS and block solution (5% FBS in PBS) was added for 30 min at 50 ^{o}C. Mucin 2 primary antibody (rabbit H-300, Santa) was diluted to 1: 200 in block solution and applied overnight at 4 ^{o}C. After washing in PBS, block solution containing anti-rabbit secondary antibody diluted to 1: 200 was applied to the section for 2 hrs. Nuclei were stained using DAPI. Observations were performed with a Zeiss LSM 700 confocal microscope with software Zen 2011 version 7.1. This software was used to determine the distance between bacteria and the epithelial cell monolayer, as well as the mucus thickness.

***Ex vivo* stimulation**

For *ex vivo* colon stimulation, colon from healthy mice were harvested, washed and incubated with or without 1×10^{9} *E. coli* in DMEM media with ATP (2 mM) for 1hr, For analyses of caspase1, caspase11 and IL-18 , the colon epithelial cells were

separated from colon tissues using 0.1% EDTA, followed by three 1 min shakings by hand, a 15-min incubation at 4 ℃, and passage through 70-μm filters (BD Falcon) to collect the flow through. Fraction containing intact and isolated crypts were collected by centrifugation at 75 g for 5 min. at 4^{o}C and washed with PBS. The lamina propria was separated from crypts to enrich for mononuclear and intestinal epithelial cells, respectively. Protein extracts were analyzed by immunoblotting for pro- and mature forms of caspase1, -11, IL-18 and IL-1β. The supernatants were collected for IL-18 ELISA. The expression of caspase1, caspase8, caspase11 and IL-18 was analyzed using immunoblotting and ELISA.

For *ex vivo* macrophage stimulation, macrophages were generated from abdomen cavity according to previously reported method (Lu et al., 2013). After ip injecting thioglycollate for 4-5 days, macrophages were collected, and then macrophages were exposed to different kinds of bacteria and collected at indicated time (3hrs or 24 hrs after stimulation). The expression of caspase1, caspase8, caspase11 and IL-18 was analyzed using immunoblotting and ELISA.

For caspase inhibition experiment, pan-caspase (100 μM), caspase1(100 μM) and caspase8 inhibitor (46 μM) were respectively added into culture, and then colon epithelial cells were separated, and expression of caspase1, caspase11 and IL-18 was analyzed using immunoblotting and ELISA.

For PKCδ inhibition experiment, PKCδ inhibitors (20μM) were added into culture, and then colon epithelial cells were separated at the indicated time. The expression of caspase1, caspase11 and IL-18 was analyzed using immunoblotting and ELISA.

Immunoprecipitation and immunoblot

Immunoprecipitation and immunoblot were performed according to previous methods (Cao et al., 2016; Su et al., 2014). The cells were lysed with cell lysis buffer (Cell Signaling Technology), which was supplemented with a protease inhibitor 'cocktail' (Calbiochem). The protein concentrations of the extracts were measured using a bicinchoninic acid assay (Pierce).

For immunoprecipitation(IP), IP was performed according to our previously method (Gao et al., 2018). The gut epithelial cells were lysed in IP lysis buffer (Pierce, Rockford, IL, USA) containing 10％ PMSF. Protein A/G magnetic beads (Pierce) were first added into the cell lysates for preclearing. The supernatant was collected after centrifuging at 12,000 rpm and then immunoprecipitated overnight at 4℃ with the anti-NLRC4 or IgG antibodies. Protein A/G Magnetic Beads Protein A/G Magnetic Beads were added into cell lysates and incubated for additional 3 hrs. After being washed with five times, lysates were denatured and resolved by SDS-PAGE gels.

For the immunoblot, hybridizations with primary antibodies were conducted for 1 h at room temperature in blocking buffer. The protein-antibody complexes were detected using peroxidase-conjugated secondary antibodies (Proteintech) and enhanced chemiluminescence (Millipore).

RT-PCR and qRT-PCR

RT-PCR and qRT-PCR were performed according to our previous methods (Cao et al., 2016; Su et al., 2014). Total RNA was extracted from the cells, tissues and organs using TRIzol reagent (Invitrogen). First-strand cDNA was generated from total RNA using oligo-dT primers and reverse transcriptase (Invitrogen Corp). The PCR products were visualized on 1.0% (wt/vol) agarose gels. Quantitative real-time PCR (qRT-PCR)

was conducted using QuantiTect SYBR Green PCR Master Mix (Qiagen) and specific primers in an ABI Prism 7000 analyzer (Applied Biosystems). GAPDH mRNA expression was detected in each experimental sample as an endogenous control. All reactions were run in triplicate. The primers used in this study were listed in the Methods.

ELISA

For the levels of TNFα, IL-1β, IL-18, IL-12 and IL-22 in mouse peripheral sera and gut tissues, ELISAs were performed according to the manufacturer's protocol. For tissue levels of cytokines, frozen tissues were homogenized in lysis buffer (PBS, 1% TritonX100 and protease inhibitor) using a Power Lyser 24 bench top bead-based homogenizer (Mobio). Lysates were centrifuged and supernatants used for ELISA.

QUANTIFICATION AND STATISTICAL ANALYSES

Two side Student's t-test and ONE-way ANOVA Bonferroni's Multiple Comparison Test were used to determine significance. The statistical significance of the survival curves was estimated using Kaplan and Meier method, and the curves were compared using the generalized Wilcoxon's test. Histological scores, bacteria copy numbers and cell numbers in different groups were analyzed by a Mann-Whitney U test. A 95% confidence interval was considered significant and was defined as $p < 0.05$. * indicates $p < 0.05$, ** $p < 0.01$, *** $p < 0.001$.

Key resources table

REAGENT or RESOURCE	SOURCE	IDENTIFIER
Antibodies for immunoblotting		

and immunostaining		
Anti-Mouse β-Actin (C4) antibody	Santa Cruz Biotechnology	Cat: sc-47778 RRID:AB_626632
FITC-Goat Anti-Rat IgG(H+L)	Proteintech	Cat: SA00003-11
Alexa Fluor 488-Goat Anti-Mouse IgG(H+L)	Proteintech	Cat: SA00006-1
Alexa Fluor 594-Goat Anti-Rabbit IgG(H+L)	Proteintech	Cat: SA00006-4
Alexa Fluor 488-Goat Anti-Rabbit IgG(H+L)	Proteintech	Cat: SA00006-2
Alexa Fluor 594-Goat Anti-Mouse IgG(H+L)	Proteintech	Cat: SA00006-3
ITC-rabbit Anti-goat IgG(H+L)	Proteintech	Cat: SA00003-4
Anti-Mouse F4/80 (3H2113)	Santa Cruz Biotechnology	Cat:sc-71088 RRID:AB_1122714
Anti-Mouse TNFalpha (52B83)	Santa Cruz Biotechnology	Cat:sc-52746 RRID:AB_630341
Anti-Mouse CD4 (EPR19514)	Abcam	Cat: ab183685 RRID:AB_2686917
Anti-Mouse IFNgamma	Abcam	Cat:ab9657 RRID:AB_2123314
Anti-Mouse IL-18	Abcam	Cat: ab71495 RRID:AB_1209302
Anti-Mouse CK19(A-3)	Santa Cruz Biotechnology	Cat:sc-376126 RRID:AB_10988034
Anti-Mouse CD11b (1B6e)	Santa Cruz Biotechnology	Cat: sc-21744 RRID:AB_626882
Anti-Mouse Caspase1	Proteintech	Cat: 22915-1-Ap
Anti-Mouse Caspase8	Proteintech	Cat: 13423-1-Ap
Anti-Mouse Caspase11 (EPR18628)	Abcam	Cat:ab180673
Anti-Mouse NLRC4	ThermoFisher	Cat:PA5-72908 RRID:AB_2718762
Anti-Mouse PKCδ	Proteintech	Cat: 19132-AP
Anti-Mouse ASC/TMS1 (D2W8U)	Cell Signaling Technology	Cat: 67824
Anti-Mouse IL-1β	ABclonal Biotechnology	Cat: A11369
Antibodies for flow cytometry		
PerCP/Cy5.5 anti-mouse CD45 (30-F11)	Biolegend	Cat:103132 RRID:AB_893340
Brilliant Violet 421™ anti-mouse CD45	Biolegend	Cat:103134 RRID:AB_2562559
PE anti-mouse MHCII (M5/114.15.2)	Biolegend	Cat:107608 RRID:AB_313323
APC anti-mouse Ly6C (HK1.4)	Biolegend	Cat:128016 RRID:AB_1732076
Brilliant Violet 605™ anti-mouse F4/80 (BM8)	Biolegend	Cat:123133 RRID:AB_2562305
APC/Cy7 anti-mouse/human CD11b (M1/70)	Biolegend	Cat: 101226 RRID:AB_830642

FITC anti-mouse CD103 (2E7)	Biolegend	Cat:121420 RRID:AB_10714791
Alexa Fluor® 700 anti-mouse CX3CR1(SA011F11)	Biolegend	Cat:149036, RRID:AB_2629606
FITC anti-mouse CD4 (RM4-5)	Thermo Fisher Scientific	Cat:11-0042-85 RRID:AB_464897
PE anti-mouse IFNgamma (XGM1.2)	Thermo Fisher Scientific	Cat:25-7311-82 RRID:AB_469680
Percp/cy5.5 anti-mouse NKp46(29A1.4)	Biolegend	Cat:137610 RRID:AB_10641137
APC anti-mouse Ki67 (SolA15)	Thermo Fisher Scientific	Cat:17-5698-82 RRID:AB_2688057
APC anti-mouse IL17 (eBio17B7)	Thermo Fisher Scientific	Cat:11-7177-81 RRID:AB_763581
PE anti-mouse Foxp3 (NRRF-30)	Thermo Fisher Scientific	Cat: 12-4771-82 RRID:AB_529580
FITC anti-mouse F4/80 (BM8)	Biolegend	Cat:123108 RRID:AB_893502
APC anti-mouse CD11c (N418)	Biolegend	Cat:117310 RRID:AB_313779
FITC anti-mouse CD11b(M1/70)	Thermo Fisher Scientific	Cat: 11-0112-82 RRID:AB_464935
APC anti-mouse TNFa (MP6-XT22)	Thermo Fisher Scientific	Cat: 17-7321-82 RRID:AB_469508
PE anti-mouse Ly6G (1A8) mouse	BD Bioscience	Cat:551461 RRID:AB_394208
FITC-Ly6C (AL-21) mouse	BD Bioscience	Cat:553104 RRID:AB_394628
Neutralizing antibody		
Mouse IL-12 Ab antibody	RD Systems	Cat: AF-419-NA RRID:AB_354485
Mouse IL-22 Ab antibody	RD Systems	Cat: AF582 RRID:AB_355457
Mouse IL-18 (93-10C) Ab antibody	RD Systems	Cat: D048-3 RRID:AB_2123796
Mouse IFNgamma (37895) Ab antibody	RD Systems	Cat: MAB485 RRID:AB_2123047
Primers for qPCR		
Murine GAPDH-Fs	BGI	5’-TCAACGGCACAGTCAAGG-3’
Murine GAPDH-Rs	BGI	5’-ACTCAGCACCGGCCTCA-3’
Murine IFNg-Fs	BGI	5’-AACGCTACACACTGCATCTTGG-3’
Murine IFNg-Rs	BGI	5’-GACTTCAAAGAGTCTGAGG-3’
Murine TNFa-Fs	BGI	5’-GGTCTGGGCCATAGAACTGA-3’
Murine TNFa-Rs	BGI	5’-CAGCCTCTTCTCATTCCTGC-3’
Murine IL-4-Fs	BGI	5’-ATCATCGGCATTTTGAACGAGG-3’
Murine IL-4-Rs	BGI	5’-TGCAGCTCCATGAGAACACTA-3’
Murine IL-6-Fs	BGI	5’-TCTGAAGGACTCTGGCTTTG-3’
Murine IL-6-Rs	BGI	5’-GATGGATGCTACCAAACTGGA-3’
Murine IL-1β-Fs	BGI	5’-GTGTCTTTCCCGTGGACCTT-3’
Murine IL-1β-Rs	BGI	5’-AATGGGAACGTCACACACCA-3’

Murine NOS-Fs	BGI	5’-TGCCCCAAGGTATCCAAGTT-3’
Murine NOS-Rs	BGI	5’-CCTCCGTCCAGTCTCCCACA-3’
Murine Arginase1-Fs	BGI	5’-CTGACCTATGTGTCATTTGGG-3’
Murine Arginase1-Rs	BGI	5’-TCAGGAGAAAGGACACAGGTT-3’
Murine IL-10-Fs	BGI	5’-AGCCTTATCGGAAATGATCCAGT-3’
Murine IL-10-Rs	BGI	5’- GGCCTTGTAGACACCTTGGT-3’
Murine IL-12-Fs	BGI	5’-TGGTTTGCCATCGTTTTGCTG -3’
Murine IL-12-Rs	BGI	5’-ACAGGTGAGGTTCACTGTTTCT -3’
Murine IL-22-Fs	BGI	5’-GCTCAGCTCCTGTCACATCA-3’
Murine IL-22-Rs	BGI	5’-CAGACGCAAGCATTTCTCAG-3’
Perimers for detection of bacteria		
16s 27F	BGI	5’- AGAGTTTGATCCTGGCTCAG-3’
16s 1492R	BGI	5’- GGTTACCTTGTTACGACTT-3’
Eubacteria-Fs	BGI	5’- ACTCCTACGGGAGGCAGCAGT-3’
Eubacteria-Rs	BGI	5’-ATTACCGCGGCTGCTGGC-3’
E. coli-Fs	BGI	5’- TGGGATCTCCATTGTCAGA-3’
E. coli-Rs	BGI	5’-CACTGGTGTGGGCCATAATTC -3’
Probe		
E.coli-Colinsitu	BGI	cy3-GAG ACT CAA GAT TGC CAG TAT CAG
Critical Commercial Assays		
Mouse IL-18 ELISA KIT	Elabscience	Cat: E-EL-M0730c
Mouse IL-1β ELISA KIT	Elabscience	Cat: E-EL-M0037c
Mouse TNFa ELISA KIT	Elabscience	Cat: E-EL-M0049c
Mouse CPK ELISA KIT	EK-Bioscience	Cat: EK-M21262
Mouse BUN ELISA KIT	EK-Bioscience	Cat: EK-M21223
Mouse ASK ELISA KIT	EK-Bioscience	Cat: EK-M20900
Mouse ALTELISA KIT	EK-Bioscience	Cat: EK-M20426
QIAquick PCR Purification Kit	Qiagen	Cat:28104
QuantiTect SYBR Green PCR Master Mix	Qiagen	Cat:208052
Foxp3 / Transcription Factor Fixation/Permeabilization Concentrate and Diluent	Thermo Fisher	Cat: 00-5521-00

Cell stimulation cocktail	ebioscience	Cat: 00-4975-03
Permeabilization Buffer	Thermo Fisher	Cat: 00-8333-56
Dual-Luciferase Reporter Assay System	Promega	Cat: E1910
ECL chemiluminescence	Absin	Cat: abs920
Protease Inhibitor Cocktail	Sigma-Aldrich	Cat: P8340
Chemicals, inhibitors		
Dextran sulfate sodium salt (DSS)	Mpbio	Cat: 160110
pan caspase inhibitor (Z-VAD-FMK)	ApexBio Technology	Cat: A1902
Caspase1 inhibitor (Z-YVAD-FMK)	ApexBio Technology	Cat: A8955
Caspase8 inhibitor(Z-IETD-FMK)	ApexBio Technology	Cat: B3232
PKCδ inhibitor (Rottlerin)	MedChemExpress	Cat: HY-18980
Ampicillin	Sigma-Aldrich	Cat: BP021
Vancomycine	Sigma-Aldrich	Cat: V2002
Neomycin sulfate	Sigma-Aldrich	Cat: N6386
Metronidazole	Sigma-Aldrich	Cat: M3761
Trizol	Life Technologies	Cat: 15596026
FBS	Gibco	Cat:10099141
Collagenase IV	Sigma-Aldrich	Cat: C5138
Dnase I	Solarbio	Cat: D8071
DMEM	Gibco	Cat:11965118
HBSS	Gibco	Cat:14170161
Pecoll	Solarbio	Cat: P8370
PMA	Sigma-Aldrich	Cat: 79346
GolgiStop	BD Biosciences	Cat: 554724
LPS	Sigma-Aldrich	Cat: L2630
7-AAD	Thermo Fisher	Cat: A1310
ATP	Sigma-Aldrich	Cat: FLAAS
EDTA	Sigma-Aldrich	Cat: 798681
Thioglycollate	Millipore	Cat: 70157
Pierce™ Protein A/G magnetic beads	Thermo Fisher	Cat: 88803

References

Bai, X., Hu, B., Xu, Y., Sun, H., Zhao, A., Ba, P., Fu, S., Fan, R., Jin, Y., Wang, H., *et al.* (2016). Molecular and Phylogenetic Characterization of Non-O157 Shiga Toxin-Producing Escherichia coli Strains in China. Front Cell Infect Microbiol *6*, 143.

Bain, C.C., Scott, C.L., Uronen-Hansson, H., Gudjonsson, S., Jansson, O., Grip, O., Guilliams, M., Malissen, B., Agace, W.W., and Mowat, A.M. (2013). Resident and pro-inflammatory macrophages in the colon represent alternative context-dependent fates of the same Ly6Chi monocyte precursors. Mucosal Immunol *6*, 498-510.

Cao, S., Su, X., Zeng, B., Yan, H., Huang, Y., Wang, E., Yun, H., Zhang, Y., Liu, F., Li, W., *et al.* (2016). The Gut Epithelial Receptor LRRC19 Promotes the Recruitment of Immune Cells and Gut Inflammation. Cell Rep *14*, 695-707.

Chassaing, B., Koren, O., Goodrich, J.K., Poole, A.C., Srinivasan, S., Ley, R.E., and Gewirtz, A.T. (2016). Corrigendum: Dietary emulsifiers impact the mouse gut microbiota promoting colitis and metabolic syndrome. Nature.

D'Haens, G., Sandborn, W.J., Feagan, B.G., Geboes, K., Hanauer, S.B., Irvine, E.J., Lemann, M., Marteau, P., Rutgeerts, P., Scholmerich, J., *et al.* (2007). A review of activity indices and efficacy end points for clinical trials of medical therapy in adults with ulcerative colitis. Gastroenterology *132*, 763-786.

DeSantis, T.Z., Brodie, E.L., Moberg, J.P., Zubieta, I.X., Piceno, Y.M., and Andersen, G.L. (2007). High-density universal 16S rRNA microarray analysis reveals broader diversity than typical clone library when sampling the environment. Microb Ecol *53*, 371-383.

Gao, Y., Sun, W., Shang, W., Li, Y., Zhang, D., Wang, T., Zhang, X., Zhang, S., Zhang, Y., and Yang, R. (2018). Lnc-C/EBPbeta Negatively Regulates the Suppressive Function of Myeloid-Derived Suppressor Cells. Cancer Immunol Res *6*, 1352-1363.

Geubel, A.P., Baggenstoss, A.H., and Summerskill, W.H. (1976). Responses to treatment can differentiate chronic active liver disease with cholangitic features from the primary biliary cirrhosis syndrome. Gastroenterology *71*, 444-449.

Liu, X., Zhan, Z., Li, D., Xu, L., Ma, F., Zhang, P., Yao, H., and Cao, X. (2011). Intracellular MHC class II molecules promote TLR-triggered innate immune responses by maintaining activation of the kinase Btk. Nat Immunol *12*, 416-424.

Lu, M., Varley, A.W., and Munford, R.S. (2013). Persistently active microbial molecules prolong innate immune tolerance in vivo. PLoS Pathog *9*, e1003339.

Ouyang, Q., Tandon, R., Goh, K.L., Pan, G.Z., Fock, K.M., Fiocchi, C., Lam, S.K., and Xiao, S.D. (2006). Management consensus of inflammatory bowel disease for the Asia-Pacific region. J Gastroenterol Hepatol *21*, 1772-1782.

Shouval, D.S., Biswas, A., Goettel, J.A., McCann, K., Conaway, E., Redhu, N.S., Mascanfroni, I.D., Al Adham, Z., Lavoie, S., Ibourk, M., *et al.* (2014). Interleukin-10 receptor signaling in innate immune cells regulates mucosal immune tolerance and anti-inflammatory macrophage function. Immunity *40*, 706-719.

Su, X., Min, S., Cao, S., Yan, H., Zhao, Y., Li, H., Chai, L., Mei, S., Yang, J., Zhang, Y., *et al.* (2014). LRRC19 expressed in the kidney induces TRAF2/6-mediated signals to prevent infection by uropathogenic bacteria. Nature communications *5*, 4434.

Tang, C., Kamiya, T., Liu, Y., Kadoki, M., Kakuta, S., Oshima, K., Hattori, M., Takeshita, K., Kanai, T., Saijo, S., *et al.* (2015). Inhibition of Dectin-1 Signaling Ameliorates Colitis by Inducing Lactobacillus-Mediated Regulatory T Cell Expansion in the Intestine. Cell Host Microbe *18*, 183-197.

Vaishnava, S., Yamamoto, M., Severson, K.M., Ruhn, K.A., Yu, X., Koren, O., Ley, R., Wakeland, E.K., and Hooper, L.V. (2011). The antibacterial lectin RegIIIgamma promotes the spatial segregation of microbiota and host in the intestine. Science *334*, 255-258.